International Journal of Environmental Science and Technology (2026) 23:269
https://doi.org/10.1007/s13762-026-07062-y

ORIGINAL PAPER

Degradation of cyclophosphamide and ibuprofen using sesame oil meal-based activated carbon composite

A. Gouran[1,2] · A. Ahmadpour[1,2] · M. Mohadesi[3]

Received: 28 April 2025 / Revised: 9 December 2025 / Accepted: 2 January 2026
© The Author(s) under exclusive licence to Iranian Society of Environmentalists (IRSEN) and Science and Research Branch, Islamic Azad University 2026

Abstract

Pharmaceutical pollutants are emerging contaminants of significant environmental concern, requiring efficient and sustainable treatment approaches. In this study, a low-cost adsorbent–photocatalyst composite synthesized from sesame oil meal waste (activated carbon@$CuFe_2O_4$@MCM-41@graphene quantum dot) was applied for the adsorption and degradation of cyclophosphamide and ibuprofen in a microphotoreactor. The composite was characterized using EDX, FT-IR, XRD, FESEM, UV–vis DRS, and BET analyses. Operating parameters including pH (2–10), composite dosage (0.1–1 g/L), pollutant concentration (5–300 mg/L for cyclophosphamide; 5–50 mg/L for ibuprofen), contact time (0.5–25 min), and temperature (25–45 °C) were evaluated. Under optimized conditions, removal efficiencies reached approximately 100% for cyclophosphamide and 98.5% for ibuprofen. The composite demonstrated good reusability, with efficiency decline becoming significant after the seventh cycle. Application to real hospital wastewater confirmed notable reductions in COD and TOC, demonstrating the practical potential of the synthesized composite for advanced wastewater treatment. Overall, this study highlights the effectiveness of a sustainable, waste-derived material integrated into a microphotoreactor system for the removal of pharmaceutical pollutants.

Editorial responsibility: Samareh Mirkia.

✉ A. Ahmadpour
ahmadpour@um.ac.ir

[1] Department of Chemical Engineering, Faculty of Engineering, Ferdowsi University of Mashhad, Mashhad 91779-48944, Iran

[2] Industrial Catalysts, Adsorbents and Environment Lab., Oil and Gas Research Institute, Ferdowsi University of Mashhad, Mashhad 91779-48974, Iran

[3] Department of Chemical Engineering, Faculty of Engineering, Kermanshah University of Technology, Kermanshah, Iran

Published online: 02 February 2026

Graphical abstract

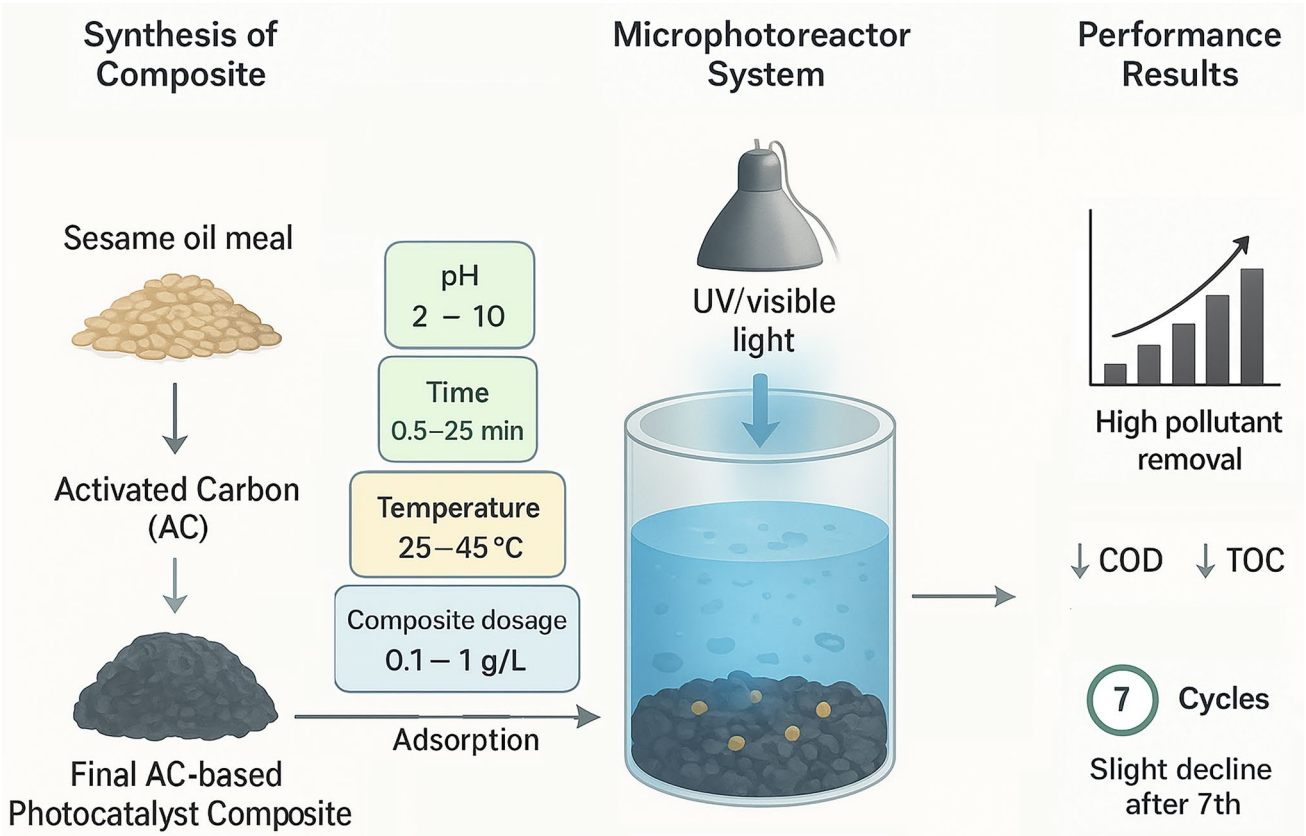

Keywords Adsorption-photocatalytic process · Aqueous solution · Pharmaceutical pollutant · Waste material

Introduction

Despite the large volume of water resources, only two percent of these resources on the planet are fresh and potable, and the rest are unusable (Lestari et al. 2025; Samimi and Moghadam 2024). Increasing human activities, including commercial and non-commercial use of pharmaceuticals, personal care products, and agricultural products, have introduced new pollutants that are challenging to remove using existing technologies (Samimi 2025; Tafreshi et al. 2024; Taj-Aldeen et al. 2024). The presence of pharmaceutical substances in water resources is very dangerous and can cause great harm to humans and natural ecosystems (Obasi et al. 2024). The highly persistent nature of pharmaceuticals makes them difficult to remove with conventional water treatment methods. It is observed that pharmaceutical pollutants accumulate in animal and plant tissues and often remain in the environment. The worrisome issue is the amount of these pollutants that end up in sewage streams as a result of their continuous use in the treatment of various diseases. Therefore, the removal of pharmaceuticals from water sources requires the development of advanced technologies that can be used in direct and indirect reuse of drinking water (Gogoi et al. 2018; Nouri Mollalar et al. 2025).

Cyclophosphamide is one of the most common cytostatic alkylating pollutants, which plays a role in the chemotherapy of various types of cancer, as well as in the treatment of autoimmune diseases, and is used as an immunosuppressant after organ transplantation (Khan et al. 2025; Lin et al. 2015). Ibuprofen is a non-steroidal anti-inflammatory pollutant that enters the environment through hospital and medical wastewater, pharmaceutical wastewater, and its use in animal husbandry and veterinary medicine. This pollutant is used to reduce fever, muscle pain, and inflammation (Mohadesi et al. 2022; Yatimzade et al. 2024).

Physical, chemical, thermal, and biological methods are usually used to remove pharmaceutical pollutants (Salameh et al. 2026). Physical methods include adsorption, electrodialysis, evaporation, dialysis, filtration, coagulation, reverse osmosis, and sedimentation (Samimi and Amiri 2024). Thermal methods include burning and pyrolysis. Activated sludge, aeration lagoon, anaerobic

digestion, and waste stabilization ponds are the most common biological methods (Gogoi et al. 2018). Activated carbons (ACs) are materials produced from carbon-rich organic materials, including coconut shells, wood, coal, peat, and other sources (Rammal et al. 2025). Adsorption using activated carbon is widely used in the removal of toxic and hazardous pollutants from the environment (Abegunde & Idowu 2023; Ezeokol et al. 2024). Activated carbon can be used to remove organic compounds from water (Ahmadi et al. 2025; Mohadesi et al. 2024). Also, rare organic chemicals, including pharmaceutical pollutants, can be oxidized using advanced oxidation processes (AOPs) (A. Alamir et al. 2024).

Due to the porosity and high surface area of activated carbon, researchers realized its importance for photocatalytic applications. The high adsorption capacity of activated carbon also enhances the electron transfer process during photocatalysis and hence increases the photocatalytic performance for degradation. Activated carbon is a valuable support material that provides synergistic effects by creating an interface between photocatalyst particles and activated carbon. Pollutant molecules are reversibly adsorbed onto the surface of activated carbon, thus increasing the efficiency of the composite compared to the photocatalyst material itself in its pure state. In photocatalytic processes, activated carbon helps to adsorb and at the same time better and more effectively decompose pollutants. Particles easily aggregate when photocatalyst is used alone, which results in the reduction of specific surface area and active sites, and they are easily degraded in aqueous solutions, making their recycling and reuse difficult. Many studies have proposed loading the catalyst onto particles with large surface area to solve these problems. Currently, the most common carriers are carbon and mesoporous materials (Wang et al. 2022; Yahya et al. 2018). However, a significant research gap persists in developing cost-effective, sustainable supports derived from agricultural waste that can effectively host complex, multi-component photocatalysts for dual-pollutant degradation. Prior studies often focus on single-component carriers or expensive precursors, lacking a critical evaluation of synergistic enhancement in practical microreactor systems.

A micro-photoreactor (MPR) is a small photoreactor that integrates the advantages of microfluidics into a conventional photoreactor. Small photoreactors for wastewater treatment require relatively small amounts of photocatalyst materials (microgram and nanogram) and offer unique features such as high surface-to-volume ratio, better control of reaction parameters, and efficient heat and mass transfer. In principle, microreactors provide uniform and consistant light distribution to the photocatalyst and homogeneous penetration throughout the depth of the microreactor. The thin photocatalyst layer in the microreactor allows less photon loss and uniform light distribution, making it suitable for photocatalytic wastewater treatment applications (Shukla et al. 2021).

Ofiarska et al. investigated the decomposition of two pollutants, ifosfamide and cyclophosphamide, using TiO_2 photocatalyst samples doped by platinum (0.15 wt%) and without doping. The results showed that the decomposition pathways of ifosfamide and cyclophosphamide are different from each other (Ofiarska et al. 2016). In a study, Osawa et al. investigated the photodegradation of cyclophosphamide and ifosfamide using ruthenium-doped titanate nanowires (Ru-TNW) in distilled water and wastewater under ultraviolet–visible (UV–vis) irradiation. Degradation pathways were suggested and both pollutants have similarities in degradation and side products (Osawa et al. 2019). In another study, Lai et al. investigated the photocatalytic degradation and conversion of ifosfamide, cyclophosphamide, and trophosphamide by TiO_2 (Lai et al. 2015). Borzyszkowska et al. used TiO_2 photocatalysts doped by Bi–B for the degradation of ifosfamide (Borzyszkowska et al. 2016). In a research, Mazierski et al. used CdS/TiO_2 nanocomposite in the photoelectrocatalytic decomposition of anticancer pollutants ifosfamide, 5-fluorouracil, and imatinib. The results have confirmed the reduction of environmental toxicity to cultivated grasses of pharmaceutical solutions treated by photoelectrocatalysis (Mazierski et al. 2023). Cyclophosphamide and ifosfamide under UV–vis/TiO_2 photocatalysis under experimental conditions were studied by Constantin et al. (Constantin et al. 2017). The obtained kinetic data confirmed that TiO_2-assisted photocatalysis was a promising method for the advanced degradation of ifosfamide and cyclophosphamide. Also, Constantin et al. studied the degradation of ifosfamide in an aqueous system through a UV–vis–Fe–TiO_2 system (Constantin et al. 2018). Haghgoo et al. used rice straw to synthesize composites based on activated carbon (AC/KOH and $AC/Fe_3O_4/ZnO$) as adsorbents to remove cyclophosphamide from water samples (Haghgoo et al. 2023).

In a study by Zendipak et al., the selective adsorption of cyclophosphamide was investigated using $Fe_3O_4@SiO_2@$ CTAB-SiO_2 nanocomposite. It was found that the maximum capacity of cyclophosphamide adsorption on the adsorbent is 342.8 mg/g (Zandipak et al. 2020). Lin et al. investigated the process of photocatalytic degradation of cyclophosphamide anticancer pollutants by UV/TiO_2 (Lin and Lin 2014). Gashtasbi et al. synthesized a magnetite composite impregnated with powdered activated carbon (PAC/Fe_3O_4) and used it to remove cephalexin from the aqueous solution through a UV system. The reusability results showed that the adsorption catalyst was usable for the cephalexin removal even after five consecutive cycles (Gashtasbi et al. 2018). In a research, Wang et al. prepared photocatalysts doped TiO_2 nanocomposites supported by powdered activated carbon with variable molar ratios for the photocatalytic degradation

of sulfamethazine (Wang et al. 2019). Silva et al. investigated the removal of sulfadiazine and oxolinic acid using magnetic biochar/titanium dioxide (BC/TiO_2) composite materials. In general, BC/TiO_2 magnetic nanocomposites are shown to be promising photocatalysts for the sustainable removal of antibiotics from aquaculture wastewater based on solar energy (Silva et al. 2021). In another study by Martins et al., a photocatalyst composed of activated carbon with TiO_2 (TiO_2/AC) was prepared and used for the degradation of tetracycline. The results showed that tetracycline was completely degraded after 75 min (Martins et al. 2017). Also, the ibuprofen removal by TiO_2-impregnated activated carbon was reported by Gu et al. Based on the results, granular activated carbon and TiO_2 composites can effectively improve the removal of ibuprofen and make the recycling process much easier and less expensive, which can be a promising method in water treatment in the future (Gu et al. 2019). Zeng et al. evaluated the photocatalytic activity of TiO_2 and TiO_2 on activated carbon (TiO_2/AC) for the degradation of amoxicillin, ampicillin, diclofenac, and paracetamol using solar radiation (Zeng et al. 2021). Pankaj et al. tested $ZnO/ZnWO_4$ nanocomposite based on activated carbon ($ZnO/ZnWO_4$/AC) for adsorption and photocatalytic degradation of oxytetracycline and ampicillin from aqueous phase under sunlight. $ZnO/ZnWO_4$/AC showed significant recyclability due to easier separation and stability in the reaction solution (Raizada et al. 2017).

In the present study, an adsorbent-photocatalyst composite activated carbon@$CuFe_2O_4$@MCM-41@graphene quantum dot (AC@$CuFe_2O_4$@MCM-41@GQD) was used to remove two pharmaceutical pollutants, cyclophosphamide and ibuprofen, in a MPR under process conditions. Operating parameters such as pH of synthetic wastewater, concentration of adsorbent-photocatalyst composite, initial concentration of pharmaceutical pollutant, time and temperature were investigated on the adsorption and degradation efficiency of the two mentioned pollutants. The primary objective of this work is to demonstrate a highly sustainable and cost-effective material derived from sesame oil meal waste that exhibits superior synergistic photocatalytic performance over pure catalysts, particularly when deployed within an efficient microreactor system. Investigations and output results show the high potential of this synthesized material in the adsorption and degradation of pharmaceutical pollutants. This approach directly addresses the critical need for sustainable advanced oxidation processes in water treatment. Degradation and removal of pharmaceutical contaminants is of great importance due to their daily hazards. In this study, a sustainable and environmentally friendly composite performed this operation well. In more detailed studies using real hospital wastewater and real environments different from the laboratory, the results well demonstrated the innovation, sustainability, and high potential of the synthesized composite. All experiments were conducted in the laboratories of Ferdowsi University of Mashhad and Kermanshah University of Technology during the summer and fall of 2023.

Materials and methods

Materials

Waste sesame oil meal was obtained from the oil production centers in Kermanshah, Iran. This material was considered as the base of activated carbon production in this study. The materials used in the synthesis of layers deposited on activated carbon are: cetyl trimethyl aluminum bromide (CTAB), ammonia solution 25%, Tetraethyl orthosilicate (TEOS), iron nitrate ($Fe(NO_3)_3{\cdot}9H_2O$) and copper acetate hydrate ($Cu(CH_3COO)_2{\cdot}H_2O$), sodium chloride (NaCl), sodium hydroxide (NaOH), citric acid ($C_6H_8O_7$), and phosphoric acid (H_3PO_4). Also, cyclophosphamide and ibuprofen pollutants were used to prepare artificial wastewater. In addition, deionized water was used in all experiments. All chemicals were obtained from Merck and Sigma-Aldrich companies.

Material synthesis

Synthesis of activated carbon

First, sesame oil meal was ground. Then, meshing and particle size separation of the powder was performed, and particles with a size less than 45 µm were considered for the preparation of activated carbon. To remove possible impurities on the particles surface, multiple washings with deionized water were performed. After that, the chemical activation was done with phosphoric acid (PA) at a weight ratio of PA to sesame oil meal powder of 1:3. In this step, the powder and phosphoric acid were mixed for 6h at a speed of 300 rpm. Then the mixture was dried in the oven. After that, the mixture was activated in a furnace under nitrogen at a temperature increase rate of 10 ºC/min from ambient temperature to 600 ºC and kept at this temperature for 2h. After cooling with the help of nitrogen flow, neutralization and washing were performed several times to reach a high effective level. Subsequently, the samples were dried and used as activated carbon for the next steps of composite synthesis (Ahmadpour and Do 1996, 1997; Qu et al. 2019).

Synthesis of MCM-41

In this study, mesoporous MCM-41 was synthesized by sol–gel method. First, a certain amount of CTAB was dissolved in deionized water at room temperature. Then, the

appropriate amount of 25% ammonia solution was added to the solution. At this stage, the pH was between 8 and 9. TEOS was then added dropwise to the solution and stirred at 300 rpm for 3h. The obtained mixture was filtered, dried, and then calcined at a temperature of 550 °C (da Costa Borges Soares et al. 2021).

Synthesis of $CuFe_2O_4$@MCM-41

First, $Cu(CH_3COO)_2{\cdot}H_2O$, $Fe(NO_3)_3{\cdot}9H_2O$, NaOH, and NaCl were combined with a molar ratio of 1:2:8:2 and stirred for 50 min at 80 ºC. Then, 1 g of MCM-41 was added to the mixture and stirred for 180 min at 60 ºC. After that, the resulting mixture was placed in an oven at 80 °C for 2h and calcined at 700 °C for 2h (da Costa Borges Soares et al. 2021).

Synthesis of GQD

Graphene quantum dot (GQD) was prepared by direct pyrolysis of citric acid. In a common method for the preparation of GQD, 2 g of citric acid was poured into a beaker and heated to 200 ºC using an oil bath. After 5 min, the color of the liquid changed from colorless to pale yellow and then to orange (within 30 min), which meant the formation of GQD (Dong et al. 2012).

Synthesis of AC@$CuFe_2O_4$@MCM-41@GQD

The composite was synthesized by combining 70 wt% of activated carbon, 25 wt% of $CuFe_2O_4$@MCM-41, and 5 wt% of GQD. First, each amount was sufficiently sonicated in deionized water using an ultrasonic bath and a homogeneous and stable solution was created.

The resulting solutions were mixed, and the final solution was subjected to sonication again for 1h at 25 ºC. Subsequently, the solution was stirred for 24h at ambient temperature at a speed of 600 rpm and then dried. The formed composite was subsequently calcined at 500 ºC in a furnace under nitrogen flow, at which point the final composite was prepared for the testing process (Jiang et al. 2018). Figure 1 shows the structure of this composite.

Characterization of synthesized materials

Characterization of the synthesized materials was carried out using Fourier transform infrared (FT-IR) analysis (Thermo Nicolet AVATAR 360) by the KBr tablet technique. X-ray diffraction (XRD) analysis (Philips PW 1730) was used to identify the chemical and crystalline composition of the materials in the 2θ range of 10.25–79.95º. The detection and determination of the surface characteristics and morphology of the synthesized materials was done by field emission scanning electron microscopy (FESEM) analysis (TESCAN model MIRA III). Zeta potential analysis (Horiba model SZ100) was used to determine the surface charge of the synthesized composite as well as the electric charge of its particles. Brunauer–Emmett–Teller (BET) analysis (BELSORP MINI II) was used to calculate the specific surface area, average pore diameter, and total pore volume of the synthesized materials. Energy dispersive X-ray (EDX) analysis (TESCAN model MIRA II with SAMX detector) was also used to determine the number of compounds and elements in the synthesized composites.

Experimental procedure

In this study, experiments were conducted in a solar microphotoreactor with an internal diameter of 600 µm and a length of 50 cm. The microreactor is placed in a wooden box surrounded by mirrors. Solar lamps (pureSunlight 1807 R 120W) were used for uniform distribution and reflection of artificial light. The MPR was placed in a water bath connected to the circulator to regulate the process temperature. The schematic of the experimental setup is shown in Fig. 2.

In the present study, the removal rate of cyclophosphamide and ibuprofen from wastewater containing these pollutants was investigated under different process conditions. The effect of various process parameters such as pH, adsorption-photocatalytic composite concentration (M), initial concentration of pharmaceutical pollutants (C_0), time (t), and temperature (T) was investigated. The range of parameters for the removal of each pollutant are listed in Table 1. Under optimal conditions, the reusability of the synthesized composite was investigated, as well as the effect of competing ions on the removal and degradation of pharmaceutical pollutants. To investigate the potential of the synthesized composite in treating real hospital wastewater, experiments were conducted under artificial light from a solar lamp as well as sunlight. The results obtained in different conditions show the high potential of the synthesized composite (AC@$CuFe_2O_4$@MCM-41@GQD) in pollutant removal. The pollutant removal percentage was calculated using Eq. 1:

$$\text{Removal}(\%) = \frac{\text{Initial concentration - Final concentration}}{\text{Initial concentration}} \times 100 \quad (1)$$

The concentration of different pollutants was determined by UV–Vis spectrometer (PG device model T80++). In order to reduce random error, all experiments were repeated three times and the average of the three results was reported.

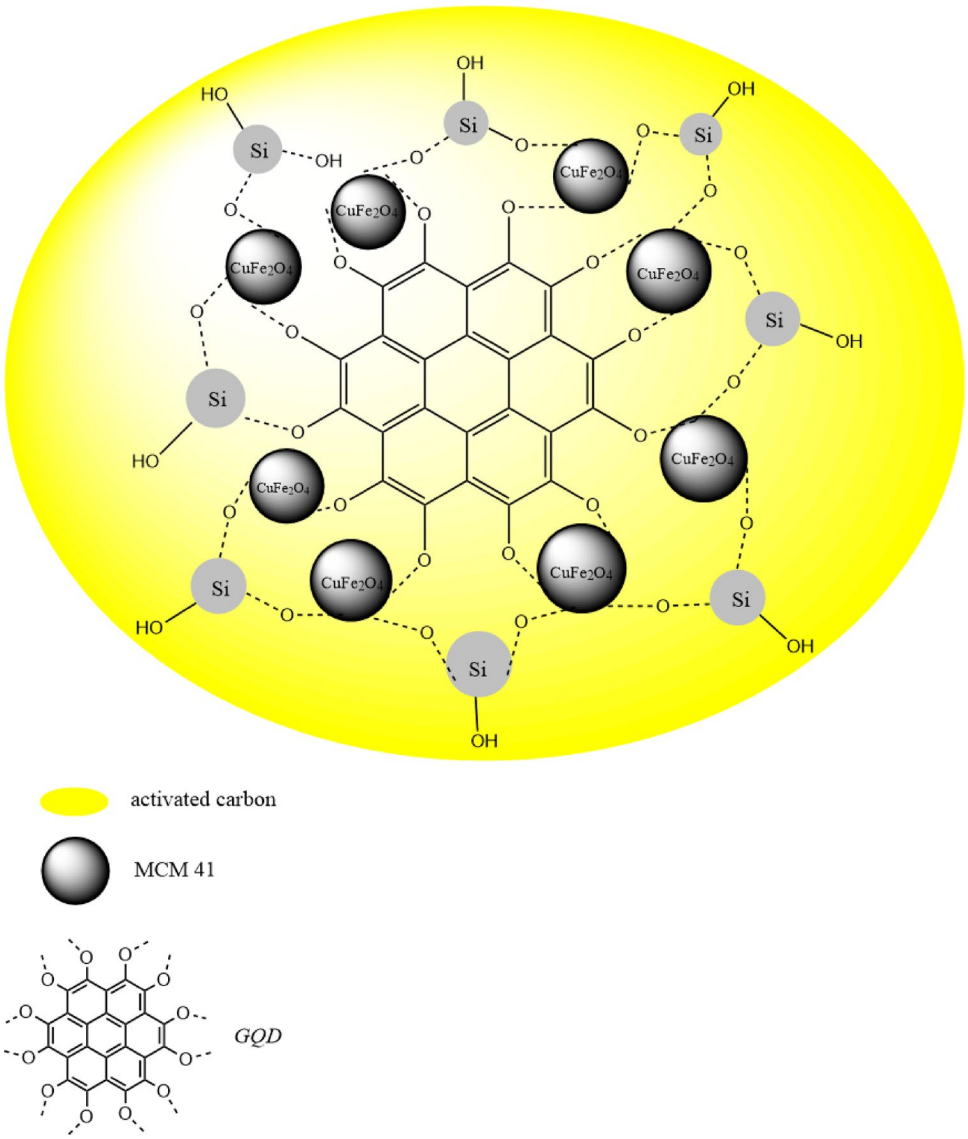

Fig. 1 Structure of AC@$CuFe_2O_4$@MCM-41@GQD composite

Results and discussion

Characterization of the synthesized composite

Elemental analysis

Using EDX analysis, the elements present in the compounds synthesized in this study were identified (see Fig. 3). The results show the proper production of activated carbon with a high percentage of carbon compared to the production source and its carbonized source. The elements in the synthesized compounds and their percentage composition are presented in Fig. 3.

FT–IR analysis

FT–IR spectrum of various synthesized compounds in the range of 400–4000 cm^{-1} was performed by KBr tablet and shown in Fig. 4. In the FT–IR spectrum of MCM-41, absorption bands of 1060 cm^{-1} and 1220 cm^{-1} related to asymmetric stretching and also 800 cm^{-1} related to symmetric stretching of Si–O groups were assigned. The band at 445 cm^{-1} shows the Si–O tetrahedral vibration mode. The broadband in the of 3455 cm^{-1} region can be attributed to the hydroxyl group of the cyanol groups as well as the absorbed water molecules (Sohrabnezhad et al. 2018).

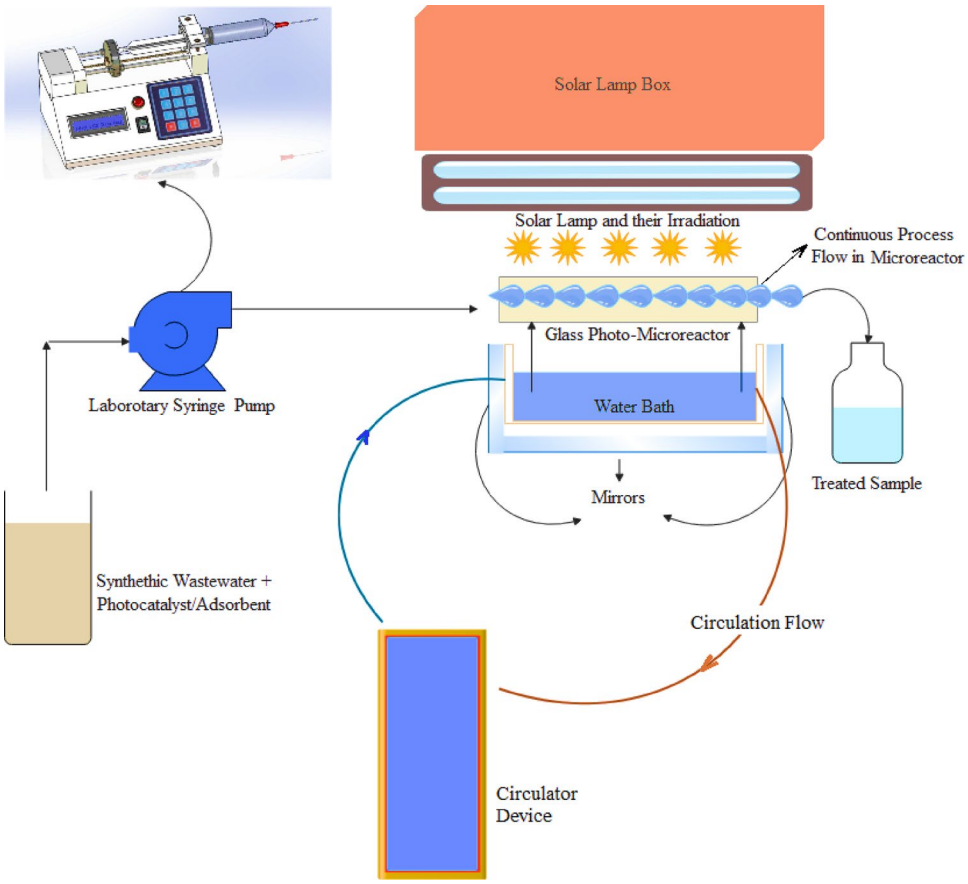

Fig. 2 Schematic diagram of the experimental setup used in this study

Table 1 The range of values of parameters investigated in this study

Pollutant	C_0 (mg/L)	M (g/L)	t (min)	T (°C)	pH
Ibuprofen	5–50	0.1–1	0.5–25	25–45	2–10
Cyclophosphamide	5–300	0.1–1	0.5–25	25–45	2–10

In the FT–IR spectrum of $CuFe_2O_4$@MCM-41 composite, the absorption bonds in the region of 557 cm^{-1}, 632 cm^{-1}, and 800 cm^{-1} correspond to the stretching peaks of the metal-oxide group, where the metal includes iron, silicon, and copper. The stretching peak in the region of 1074 cm^{-1} is related to the Si–O–Si group. Also, the bending peak in the region of 1213 cm^{-1} belongs to the Si–O–Si group. The absorption band in the 1619 cm^{-1} region corresponds to the bending peak of the hydroxyl group. The absorption band in the 3411 cm^{-1} region can be attributed to the hydroxyl group of the cyanol groups or absorbed molecules (Jermy et al. 2021, 2019).

In the FT-IR spectrum of activated carbon, the broad peak at about 3456 cm^{-1} corresponds to the bands of the O–H group due to the vibration of water molecules. The peak in the region of 2923 cm^{-1} is attributed to the presence of aliphatic C–H stretching of CH, CH_2, and CH_3 groups. The peak at 2852 cm^{-1} is related to the symmetric stretching of CH_2. The peak in the 1569 cm^{-1} region also corresponds to the C=O stretch of carboxylic acids. The 1421 cm^{-1} band is related to asymmetric and symmetric C–H bending vibrations. The weak band in the range between 900 cm^{-1} and 1100 cm^{-1} is due to the presence of the C–O group in the sample. Also, the observed band at 873 cm^{-1} corresponds to the stretching vibrations band of the C-H (Budinova et al. 2006; Xu et al. 2014).

In the FT-IR spectrum of the synthesized composite (AC@$CuFe_2O_4$@MCM-41@GQD), the broad peak around 3480 cm^{-1} related to the O–H bands of water molecules, the peak of 2920 cm^{-1} attributed to the presence of aliphatic C–H stretching of CH, CH_2, and CH_3 groups, and the peak at 2850 cm^{-1} assigned to the symmetric stretching of CH_2 are also observed. The peak in the region of 1590 cm^{-1} can be related to the C=O stretching of carboxylic acids. The 1410 cm^{-1} band related to asymmetric and symmetric C–H bending vibrations and the weak band in the range of 900 cm^{-1} to 1100 cm^{-1} due to the presence of the C–O group in the sample can be seen. Also, the band found at 874 cm^{-1} corresponds to the stretching vibrations of the C–H band. The stretching peak in regions of 571 cm^{-1}, 611 cm^{-1}, and 815 cm^{-1} corresponds to the stretching peak of Cu–O and Fe–O. The stretching and bending peaks in the region of 1067 cm^{-1} and 1096 cm^{-1} are related to Si–O–Si.

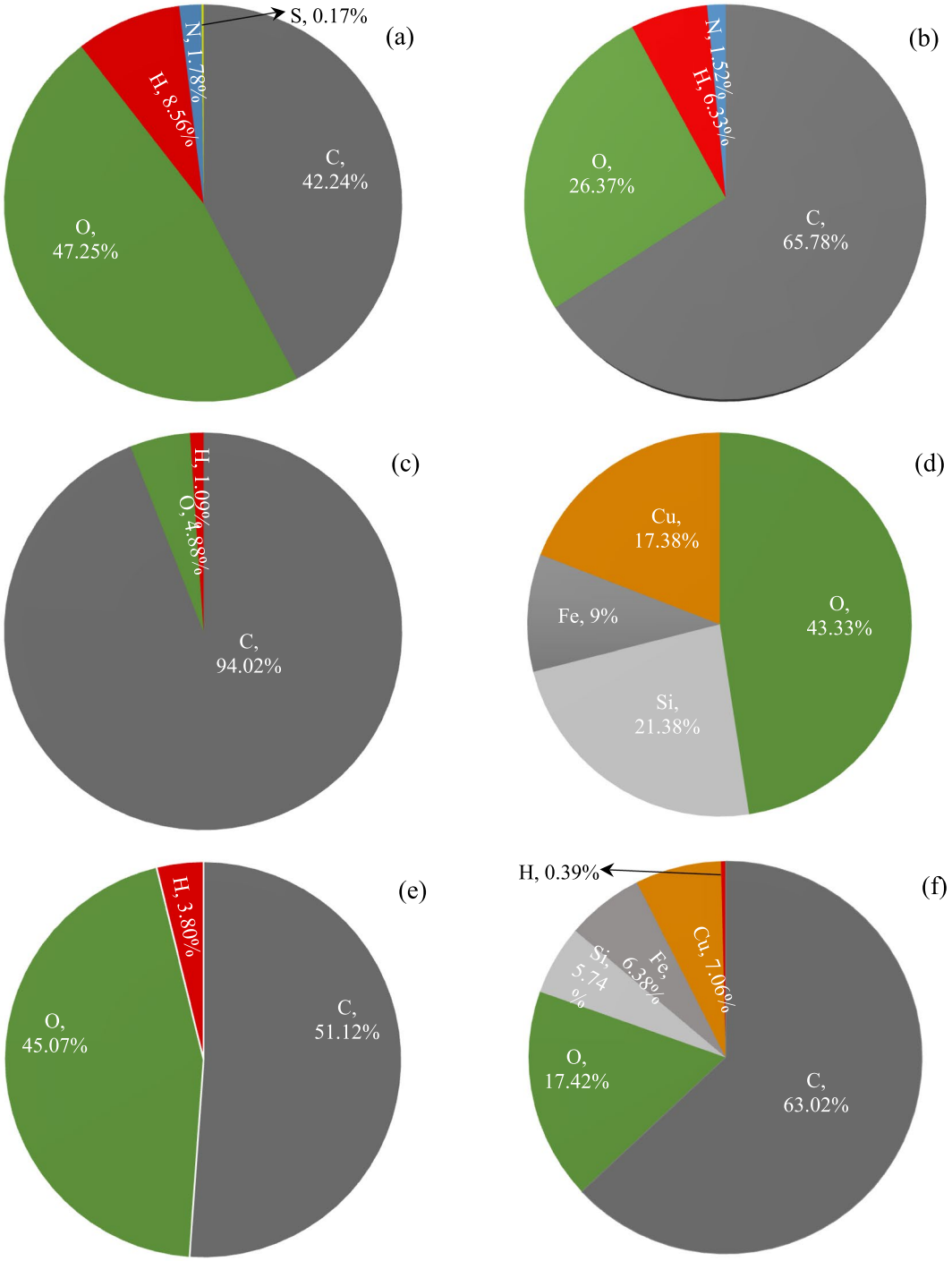

Fig. 3 Elemental analysis of the synthesized compounds; **a** sesame oil meal, **b** carbonized material, **c** activated carbon, **d** $CuFe_2O_4$@MCM-41, **e** GQD, and **f** AC@ $CuFe_2O_4$@MCM-41@GQD

XRD analysis

The X-ray diffraction pattern for the synthesized compounds is plotted in Fig. 5. As it is clear in the X-ray diffraction pattern for MCM-41, the crystal structure of the sample has characteristic peaks in the region of 2θ equal to 22.85° and 42.25°. The characteristic peaks of the XRD pattern for MCM-41 are consistent with the reported results. The model number for MCM-41 is JCPDS 00-049-1712; which shows the successful synthesis of semi-porous silica material (Lashaki et al. 2022; Pham et al. 2020).

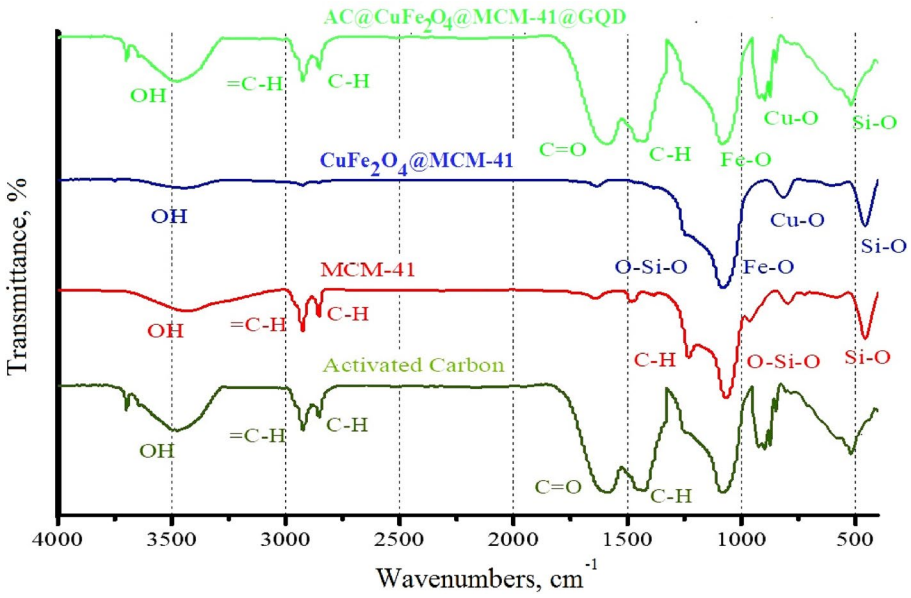

Fig. 4 FT-IR spectrum of the synthesized compounds

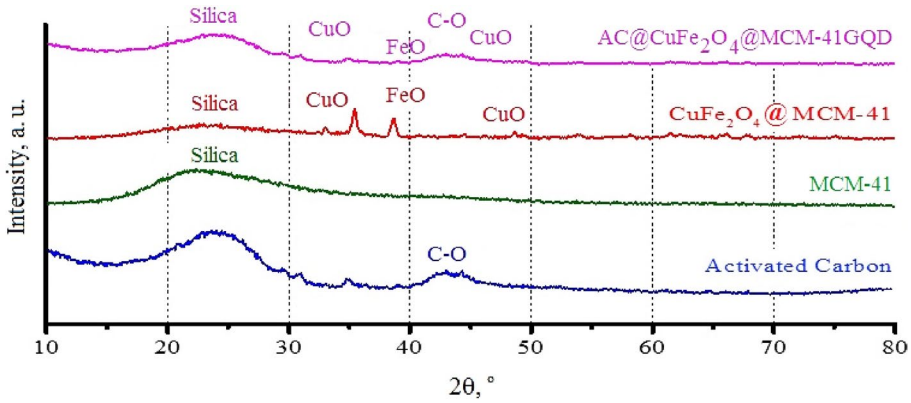

Fig. 5 X-ray diffraction pattern of the synthesized compounds

Based on the XRD results for $CuFe_2O_4$@MCM-41, the crystal structure of the sample has peaks in the 2θ region equal to 15–35º, 33.20º, 35.20º, 38.72º, 48.70º, 57.10º, and 63.20º (Shamsuddin et al. 2016). The characteristic peaks of the XRD pattern for $CuFe_2O_4$@MCM-41 are consistent with the reported results. Model numbers for $CuFe_2O_4$ and MCM-41 are JCPDS 34–0425 and JCPDS 00–049–1712, respectively. The results obtained from the XRD pattern show that the ferrite material has a crystalline structure and the characteristic peaks of the semi-porous silica material have appeared in the spectrum; which shows the successful synthesis of $CuFe_2O_4$@MCM-41 compound (Jermy et al. 2021, 2019; Shamsuddin et al. 2016).

Based on the XRD results for activated carbon, the crystalline structure of the sample has peaks of 25.25º, 35.25º, and 44.40º. The characteristic peaks of XRD patterns for carbon are consistent with the reported results. The pattern number for the carbon is JCPDS 721616. As the X-ray diffraction pattern shows, it indicates the successful synthesis of activated carbon (Prahas et al. 2008; Shamsuddin et al. 2016).

The XRD pattern for the synthesized composite (AC@$CuFe_2O_4$@MCM-41@GQD) was investigated at the lower angles of the sample. The intensity of the peaks of the composite has decreased compared to the precursor compounds alone. The reason can be attributed to the decrease in the amount and crystallinity of the composite, which is caused by adding them to each other. According to the XRD results, the crystal structure of the sample has 2θ equal to 24.50º, 35.10º, 38.72º, 48.70º, 57.10º and 63.20º. The XRD pattern of the synthesized composite has characteristic peaks of all the precursor materials and therefore the composite is properly synthesized.

FESEM analysis

High resolution FESEM was used to determine the size distribution of the synthesized nanoparticles and to characterize

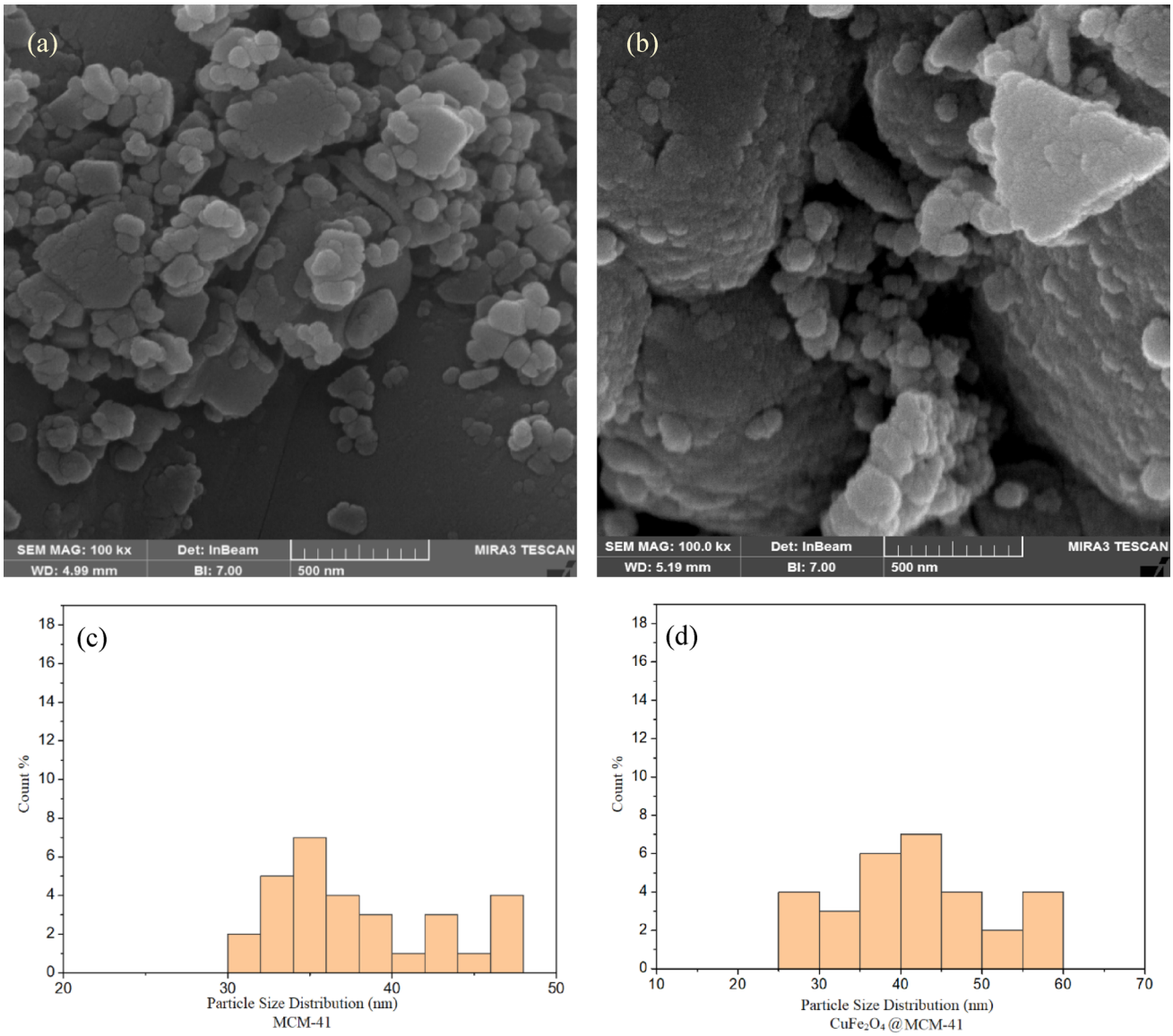

Fig. 6 SEM images and particle size distribution diagrams; **a** and **b** MCM-41, **c** and **d** MCM-41@$CuFe_2O_4$

them. The results of electron microscope images for MCM-41, $CuFe_2O_4$@MCM-41, activated carbon, and AC@$CuFe_2O_4$@MCM-41@GQD are presented in Figs. 6 and 7.

Figure 6a shows the electron microscope image of MCM-41 at 500 nm magnification. In general, the particles are arranged in spherical or inclined hexagonal frameworks. Therefore, the image clearly shows the formation of MCM-41 and the porosity of the structure can be seen well. Also, the particle size distribution of this material is in the range of 30–50 nm, and a large part of this compound has a particle size of about 35 nm (see Fig. 6b).

Figure 6c shows the SEM image of MCM-41 modified by copper ferrite. Compared to Fig. 6a (MCM-41), changes in the material structure are seen. Surface modification and the introduction of copper ferrite into MCM-41 caused several particles to come together and become slightly lumpy and out of order. The particle size distribution varies from 25 to 60 nm, with most of them in the range of 35–45 nm (see Fig. 6d). Compared to MCM-41, the particle size is slightly increased, which is due to the presence of copper ferrite groups.

Figure 7a is related to the synthesized activated carbon. The SEM image shows the successful synthesis of this material. The particle size distribution is between 100 and 110 nm, with a significant value around 107 nm (see Fig. 7c).

Figure 7b shows the SEM image of the synthesized composite (AC@$CuFe_2O_4$@MCM-41@GQD). The surface roughness increased and can be related to the incorporation of $CuFe_2O_4$ and MCM-41. The particle size increased and

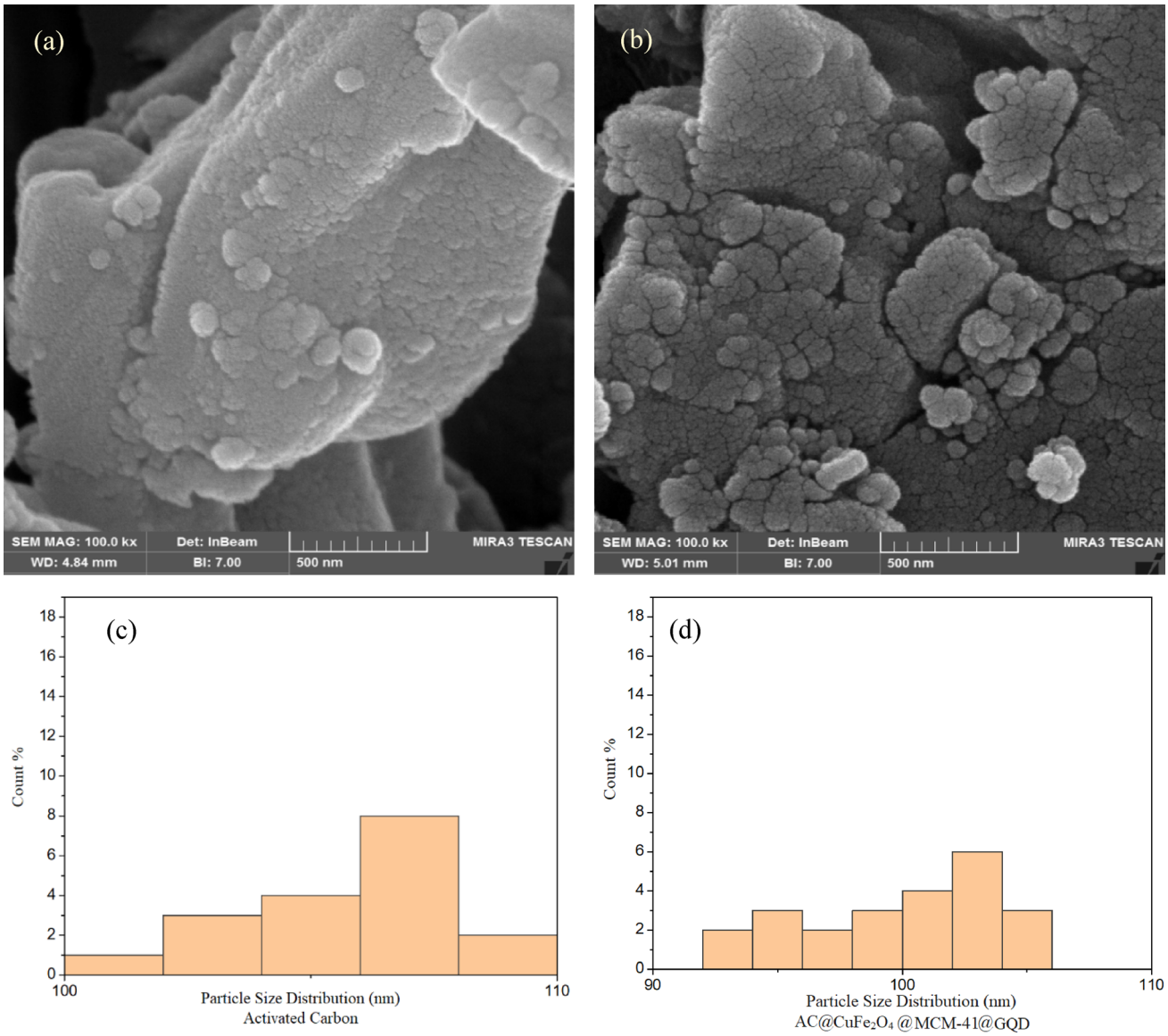

Fig. 7 SEM images and particle size distribution diagrams; **a** and **c** synthesized activated carbon, **b** and **d** synthesized composite in this study (AC@$CuFe_2O_4$@MCM-41@GQD)

this is due to the combination of these two compounds and the formation of a single material. The particle size distribution is in the range of 95–105 nm (see Fig. 7d).

UV–Vis diffuse reflectance spectroscopy (DRS) analysis

The UV–Vis diffuse reflectance spectroscopy results for the synthesized compounds are shown in Fig. 8. In the UV region, the maximum wavelength for MCM-41, $CuFe_2O_4$@MCM-41, GQD, and AC@$CuFe_2O_4$@MCM-41@GQD were observed at 320, 247, 296, 336, and 296 nm, respectively. At these values, the absorption intensities were 0.631, 0.921, 1.212, 1.222, and 1.021, respectively.

The results show an increase in the adsorption intensity of the synthesized composite compared to activated carbon, which indicates its successful synthesis and correct loading of the photocatalytic layers on the activated carbon. These observations indicate the incorporation of the photocatalytic layers into the activated carbon structure during the ion exchange process. The presence of GQD is also well demonstrated by the gradient changes in the structure of the synthesized composite at 200–250 nm. Using the relationship $E = \frac{hc}{\lambda}$, the bond gap energy for the synthesized composite was found to be 4.25 eV. In this equation, h is Planck's constant and is equal to 6.626×10^{-34} J.s, c is the speed of light and is equal to 3×10^8 m/s, λ is the maximum wavelength in nm and 1 eV is equal to 1.6×10^{-19} J.

BET analysis

Table 2 shows the volume of gas adsorbed in the standard state, specific surface area, total pore volume, and average pore diameter of all synthesized compounds. The average pore diameter of activated carbon, MCM-41, $CuFe_2O_4$@MCM-41, and AC@$CuFe_2O_4$@MCM-41@GQD are 4.591, 5.988, 4.972, and 5.988 nm, and the total pore volume are about 0.474, 0.758, 0.668, and 0.758 cm^3/g, respectively. N_2 desorption increased above 0.95 and reached a maximum value. The specific surface area of the synthesized activated carbon, MCM-41, $CuFe_2O_4$@MCM-41, and AC@$CuFe_2O_4$@MCM-41@GQD were obtained to be 1125.0, 946.5, 537.2, 548.8 m^2/g, respectively, which are good values compared with similar works (see Table 3).

According to the reported results, the specific surface area and total pore volume have decreased compared to MCM-41. According to the FESEM images, it can be interpreted that the agglomeration and proximity of the particles to each other has reduced the specific surface area and total pore

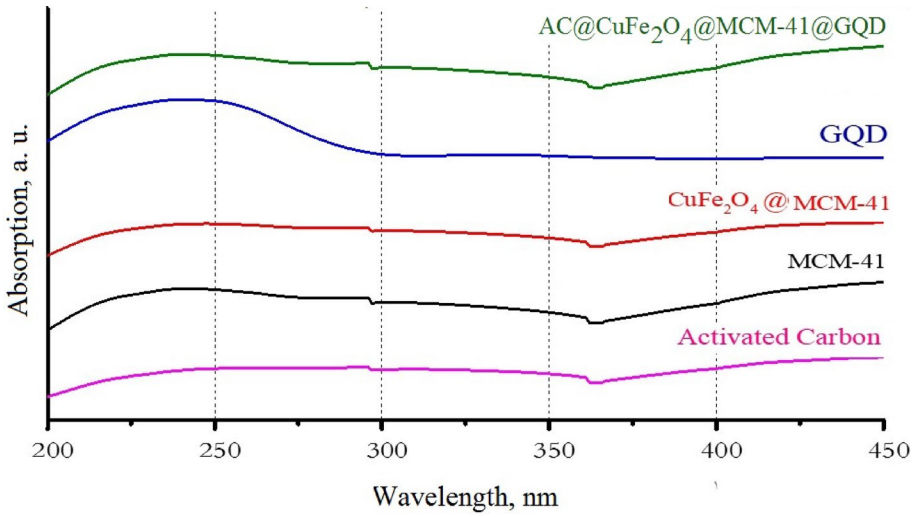

Fig. 8 UV–vis dispersive reaction spectroscopy of the synthesized compounds

Table 2 BET analysis results of the synthesized compounds

Compound	V_m (cm^3 STP/g)	$a_{s,BET}$ (m^2/g)	Total pore volume (cm^3/g)	Average pore diameter (nm)	Porosity (%)
Activated carbon	257.98	1125.0	0.474	4.591	87.56
MCM-41	217.47	946. 5	0.758	5.936	95.16
MCM-41@$CuFe_2O_4$	123.42	537.2	0.668	4.972	80.55
AC@$CuFe_2O_4$@MCM-41@GQD	126.11	548.8	0.784	5.988	84.63

Table 3 Specific surface area of activated carbon synthesized from different materials

Precursor	$a_{s,BET}$ (m^2/g)	Refs.
Spent coffee ground (Arabica)	721	(Zięzio et al. 2020)
Apple waste	854	(Hesas et al. 2013)
Cotton stalks	1032	(Nahil & Williams 2012)
Palm shells	1109	(Lim et al. 2010)
Sesame oil meal	1125	This study
Almond shells	1128	(İzgi et al. 2019)
Pecan shell	1130	(Guo & Rockstraw 2007b)
Grape seeds	1139	(Al Bahri et al. 2012)
Olive stones	1218	(Yakout & El-Deen 2016)
Eucalyptus camaldulensis Dehn bark	1239	(Patnukao & Pavasant 2008)
Jackfruit peel waste	1260	(Prahas et al. 2008)
Rice hull	1295	(Guo & Rockstraw 2007a)

volume. Comparison of the BET analysis results of MCM-41 and $CuFe_2O_4$@MCM-41 shows the successful synthesis of MCM-41 with copper ferrite and is generally in accordance with the IUPAC rules for semi-porous materials. As the results show, with the combination of materials and the synthesized composite, the specific surface area and average pore diameter decreased. Both values are significantly reduced compared to activated carbon and $CuFe_2O_4$@MCM-41. The reason for this decrease can be attributed to the composite of these two compounds. However, in general, the final synthesized composite is in the range of porous compounds. This material plays a fundamental role in the adsorption of pollutant compounds and their photocatalytic degradation in the presence of sunlight.

Effect of operating parameters on the removal and destruction efficiency of pharmaceutical pollutants

Effect of pH

According to the zeta potential analysis of the synthesized composite, the pHiso is 5.34 (see Fig. 9). When the pH of the solution is higher than this value, the surface of the synthesized composite has a negative charge, and when it is lower, the surface has a positive charge. This property affects the adsorption or desorption of pollutants under different acidic and basic conditions.

Cyclophosphamide is a weak base with a pKa of 4.9. At pH values below 4.9, it will be protonated and carry a positive charge. At pH values above 4.9, it will be deprotonated and neutral. Conversely, ibuprofen is a weak acid with a pKa of 4.52. At pH values below 4.52, it will be protonated and neutral, while at pH values above 4.52, it will be deprotonated and carry a negative charge. The pKa value represents the pH at which 50% of the molecules are protonated and 50% are deprotonated. At pH values significantly below the pKa, the molecule will be predominantly protonated, while at pH values significantly above the pKa, the molecule will be predominantly deprotonated. Cyclophosphamide is an organophosphorus compound with a complex cyclic structure. Ibuprofen is a propionic acid derivative. The chemical structures of these compounds are readily available in standard chemistry textbooks and online databases.

The effect of pH on the removal and degradation efficiency of pharmaceutical pollutants was investigated for each of the pollutants under constant process conditions and only changing the pH in the range of 2–10. To adjust the pH of the solutions according to the value of this parameter, NaOH and HCl with a concentration of 0.1 M were used for each experiment. For cyclophosphamide, the values of constant parameters were: $C_0 = 40$ mg/L, $M = 0.5$ g/L, $t = 8$ min, and $T = 25$ °C; and for ibuprofen these parameters were: $C_0 = 20$ mg/L, $M = 0.5$ g/L, $t = 9$ min and $T = 25$ °C. Under the mentioned conditions, the effect of pH was investigated in the MPR (see Fig. 10).

For ibuprofen, the pKa value is 4.52. According to this value and the pH_{iso} of the synthesized composite, the photocatalytic removal and degradation takes place. Due to the repulsion and attraction created in different ranges of pH value, different efficiencies of the composite performance in the removal and degradation of ibuprofen are observed. The highest removal efficiency of ibuprofen at pH = 5 was 86.55% and the lowest removal of cyclophosphamide at pH = 10 was 22.33% (see Fig. 10). The reason for the chang in these values is the strength of attraction and repulsion and the decrease or increase in its intensity at different pH points (Khan et al. 2019; Kumar et al. 2018; Tanveer et al. 2019; Yilmaz et al. 2020).

Effect of initial concentration of pollutants

Under constant process conditions (pH, concentration of adsorption-photocatalytic composite, time, and temperature), the effect of the initial concentration of pharmaceutical pollutants on the removal percentage of these pollutants was investigated. The removal and degradation of

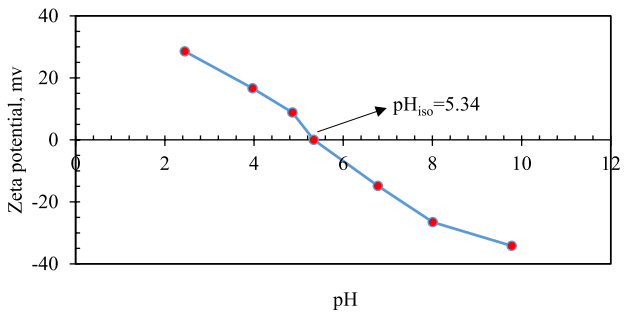

Fig. 9 The effect of pH on the zeta potential of AC@$CuFe_2O_4$@MCM-41@GQD composite

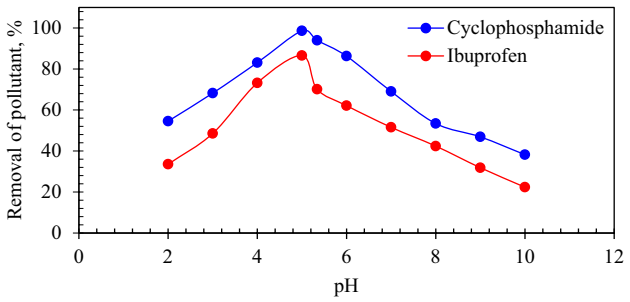

Fig. 10 Effect of pH on pollutants removal by AC@$CuFe_2O_4$@MCM-41@GQD (cyclophosphamide: $C_0 = 40$ mg/L, $M = 0.5$ g/L, $t = 8$ min, and $T = 25$ °C; ibuprofen:$C_0 = 20$ mg/L, $M = 0.5$ g/L, $t = 9$ min, and $T = 25$ °C)

cyclophosphamide was investigated under constant process conditions of pH = 5, M = 0.5 g/L, t = 8 min, and T = 25 °C in the initial concentration range of 5–300 mg/L. As shown in Fig. 11a, by increasing the initial concentration of cyclophosphamide in wastewater, the removal efficiency decreases due to the reduction of the capacity and potential of the composite. Therefore, the maximum removal of cyclophosphamide for the initial concentration of 5 mg/L was 99.98% and the lowest value was 12.24% at 300 mg/L.

Also, for ibuprofen, the effect of the initial concentration of 5–50 mg/L on the removal and degradation of this pollutant under constant process conditions of pH = 5, M = 0.5 g/L, t = 9 min, and T = 25 °C was investigated. As the initial concentration of ibuprofen increases, the removal and destruction of this pollutant decreases because the potential of the composite at constant conditions decreases due to the increased presence of pollutant molecules. The capacity and active sites of the composite are fixed and for a given amount of pollutant it has more space to trap and degrade. As the pollutant concentration increases, after this capacity is filled and its degradation potential decreases, the removal and degradation efficiency decreases. For the removal and degradation of ibuprofen, the highest efficiency of 94.85% was obtained at an initial concentration of 5 mg/L. Meanwhile, the lowest removal and degradation efficiency of 30.12% was obtained for this substance at an initial concentration of 50 mg/L (see Fig. 11b) (Di et al. 2017; Janssens et al. 2019; Kumar et al. 2018; Lin & Lin 2014).

Effect of composite concentration

By increasing the concentration of the absorption-photocatalytic composite in the wastewater solution, more sites are provided for adsorption and, consequently, more potential for the removal and destruction of pharmaceutical pollutants. In other words, by increasing the concentration of the composite, the capacity of the composite for a given amount of pollutant in the wastewater increases.

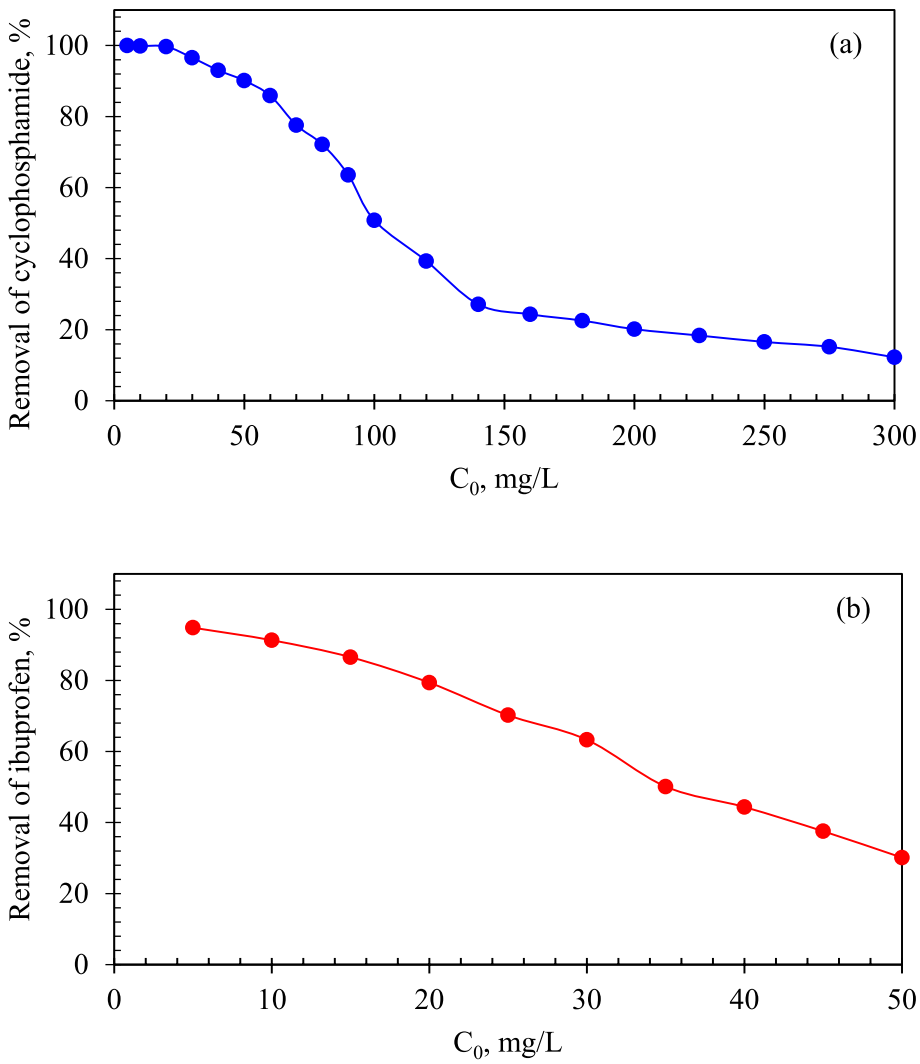

Fig. 11 Effect of initial concentration on pollutants removal by AC@$CuFe_2O_4$@MCM-41@GQD; **a** cyclophosphamide (pH = 5, M = 0.5 g/L, t = 8 min, and T = 25 °C), **b** ibuprofen (pH = 5, M = 0.5 g/L, t = 9 min, and T = 25 °C)

The effect of adsorption-photocatalytic composite concentration under constant process conditions (pH = 5, C_0 = 40 mg/L, t = 8 min, and T = 25 °C) on cyclophosphamide removal was investigated in the composite concentration range between 0.1–1 g/L. According to the results, it was found that increasing the composite concentration significantly increased the removal and degradation efficiency of cyclophosphamide. Therefore, at a composite concentration of 1 g/L, the removal efficiency was approximately 100%, which is the highest efficiency in the process conditions. Also, the lowest removal efficiency was obtained at a composite concentration of 0.1 g/L, equivalent to 48.55% (see Fig. 12). Also, the effect of composite concentration under constant process conditions (pH = 5, C_0 = 20 mg/L, t = 9 min, and T = 25 °C) was investigated for the removal of ibuprofen in the composite concentration range between 0.1 and 1 g/L. With increasing composite concentration, the removal and degradation efficiency of ibuprofen increased. At a composite concentration of 0.1 g/L, the lowest removal efficiency was obtained with 35.12%. The highest removal efficiency was obtained with increasing composite concentration under constant process conditions at a composite concentration of 1 g/L equivalent to 30%. The upward trend of increasing removal and degradation efficiency of ibuprofen with increasing composite concentration is seen in Fig. 12 (Haghgoo et al. 2023; Janssens et al. 2019; Khan et al. 2019; Kumar et al. 2018; Lin & Lin 2014; Tanveer et al. 2019; Yilmaz et al. 2020; Zandipak et al. 2020)

Effect of time and temperature

Temperature is one of the parameters that can be investigated for the removal and photocatalytic degradation of pollutants. For cyclophosphamide and ibuprofen in the range of 25–45 ºC and time of 0.5–25 min, changes in the removal efficiency and photocatalytic degradation of pollutants were investigated under constant process conditions of other variables (pH, initial concentration of the pharmaceutical pollutants, and concentration of the adsorption-photocatalytic composite). The results show that the removal and degradation efficiency increases with increasing time at all temperatures studied. Also, increasing time under constant process conditions (temperature and other parameters) provides more opportunity for bond formation and adsorption of pharmaceutical pollutant molecules. In other words, by increasing the time, the adsorption capacity and potential of the adsorbent-photocatalyst composite can be utilized to a greater extent. Also, by increasing the time of continued pollutant adsorption, the photocatalytic degradation increases, which is due to having more time for the high-energy excited photons from the surface of the photocatalytic compounds to attack the target pollutants and destroy them. For both pharmaceutical pollutants (cyclophosphamide and ibuprofen), the photocatalytic removal and degradation efficiency increased with increasing temperature. This increase was more visible and noticeable in a short period. For both pollutants, efficiencies higher than 99% were achieved with increasing time (see Fig. 13) (Janssens et al. 2019; Lin & Lin 2014).

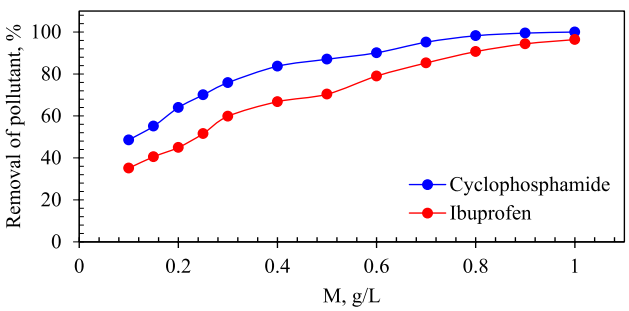

Fig. 12 Effect of composite concentration on pollutants removal by AC@$CuFe_2O_4$@MCM-41@GQD (cyclophosphamide: pH = 5, C_0 = 40 mg/L, t = 8 min, and T = 25 °C; ibuprofen: pH = 5, C_0 = 20 mg/L, t = 9 min, and T = 25 °C)

Effect of time and initial concentration of pharmaceutical pollutants

As can be seen in Fig. 14, under the condition of constant initial concentration of pharmaceutical pollutants, with increasing time, the photocatalytic adsorption composite can have an opportunity to use its full capacity to remove and destroy pharmaceutical pollutants. Also, with increasing initial concentration of pharmaceutical pollutants under constant process conditions (time and other variables), the efficiency decreases (due to the increase in the potential of the adsorbent-photocatalyst composite with reducing initial concentration of pollutants). With the simultaneous increase in the initial concentration of pharmaceutical pollutants, the efficiency of removing and eliminating pollutants decreases. With the passage of time, the efficiency of pollutant removal and destruction increases and eventually, at the time of equilibrium, the removal and destruction rate of pollutants becomes constant (Di et al. 2017; Haghgoo et al. 2023; Janssens et al. 2019; Khan et al. 2019; Kumar et al. 2018; Li et al. 2016; Lin & Lin 2014; Tanveer et al. 2019; Yilmaz et al. 2020).

Effect of time and light

To investigate the effect of light on the removal of pharmaceutical pollutants, experiments were conducted both in the presence and absence of artificial solar radiation. The solar lamp used in this study (pureSunlight 1807 R 120W) emits light in the 250–400 nm range, with a spectrum similar to natural sunlight. The band gap energy of the synthesized

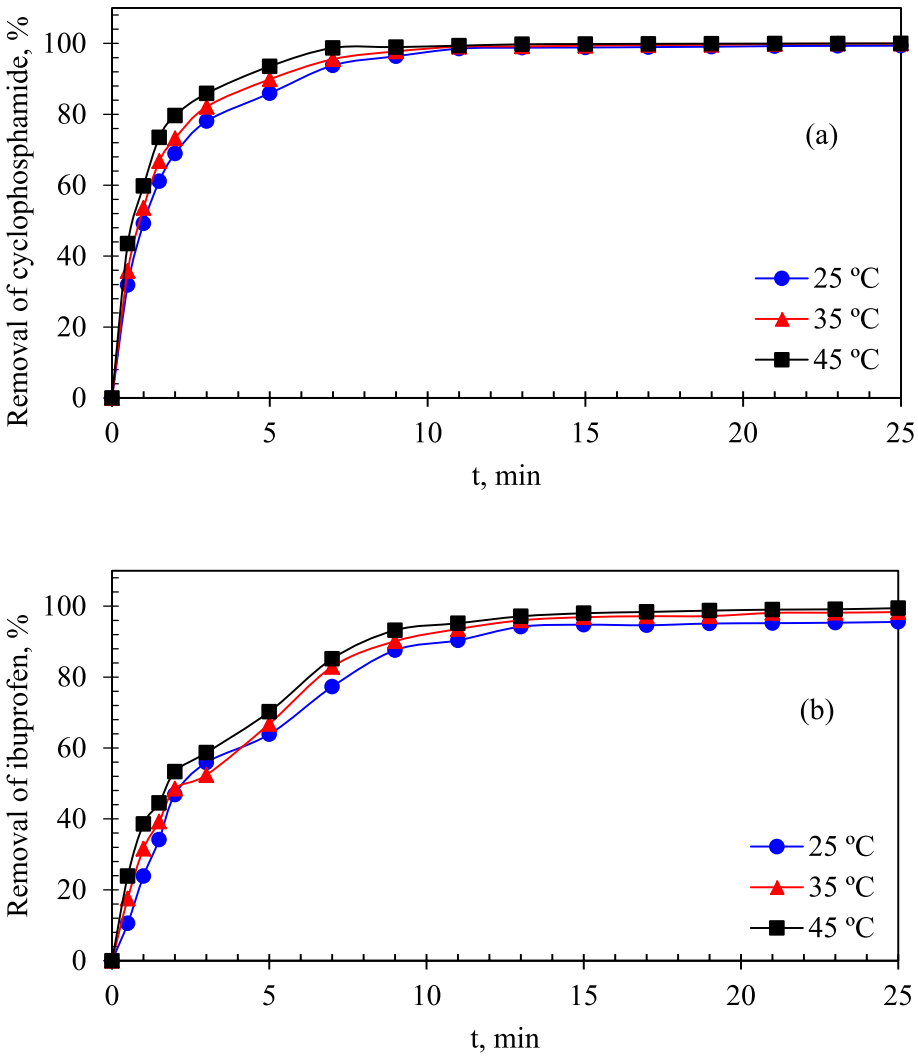

Fig. 13 Effect of time and temperature on pollutants removal by AC@$CuFe_2O_4$@MCM-41@GQD; **a** cyclophosphamide (pH = 5, C_0 = 40 mg/L, and M = 0.5 g/L), **b** ibuprofen (pH = 5, C_0 = 20 mg/L, and M = 0.5 g/L)

composite is 4.25 eV, which corresponds to a wavelength of approximately 292 nm. Therefore, the solar lamp provides sufficient energy to excite the photocatalyst. As shown in Fig. 15, the synthesized composite exhibited a significant difference in removal efficiency under light irradiation compared to dark conditions. Therefore, the synthesized composite showed a significant difference in the removal and degradation of pharmaceutical pollutants under light irradiation and without light irradiation. The removal and desgradation efficiency of cyclophosphamide was investigated under the optimal process conditions (pH = 5, C_0 = 40 mg/L, M = 0.5 g/L and T = 25 °C) and under several conditions (using the composite in the presence of solar light, using the composite in a dark box, using activated carbon in a dark box, using $CuFe_2O_4$@MCM-41 in a dark box, and using $CuFe_2O_4$@MCM-41 in the presence of a solar lamp) (see Fig. 15a).

As the results in Fig. 15a show, the removal and destruction efficiency of cyclophosphamide is close to 100% for the composite only using the solar lamp. This indicates the suitability of the synthesized composite for the removal and elimination of cyclophosphamide from synthetic wastewater. In the absence of solar light, the synthesized composite has a 15–20% lower efficiency in the removal of cyclophosphamide under the same conditions, which is due to the absence of photocatalytic materials under these conditions. The results also show that the composite synthesized in the dark box can achieve acceptable performance over a longer period of time. Activated carbon can remove and decompose cyclophosphamide in a dark box, about 25–35% less than the adsorbent-photocatalytic composite. Under the same process conditions, the $CuFe_2O_4$@MCM-41 composite was investigated in a dark box under the presence of a solar lamp. The results show a decrease in the efficiency of cyclophosphamide removal and degradation compared to the AC@$CuFe_2O_4$@MCM-41@GQD composite (in the dark box, a 75–80% reduction, and in the presence of a solar lamp, a 40–45% reduction in cyclophosphamide removal and degradation occurred).

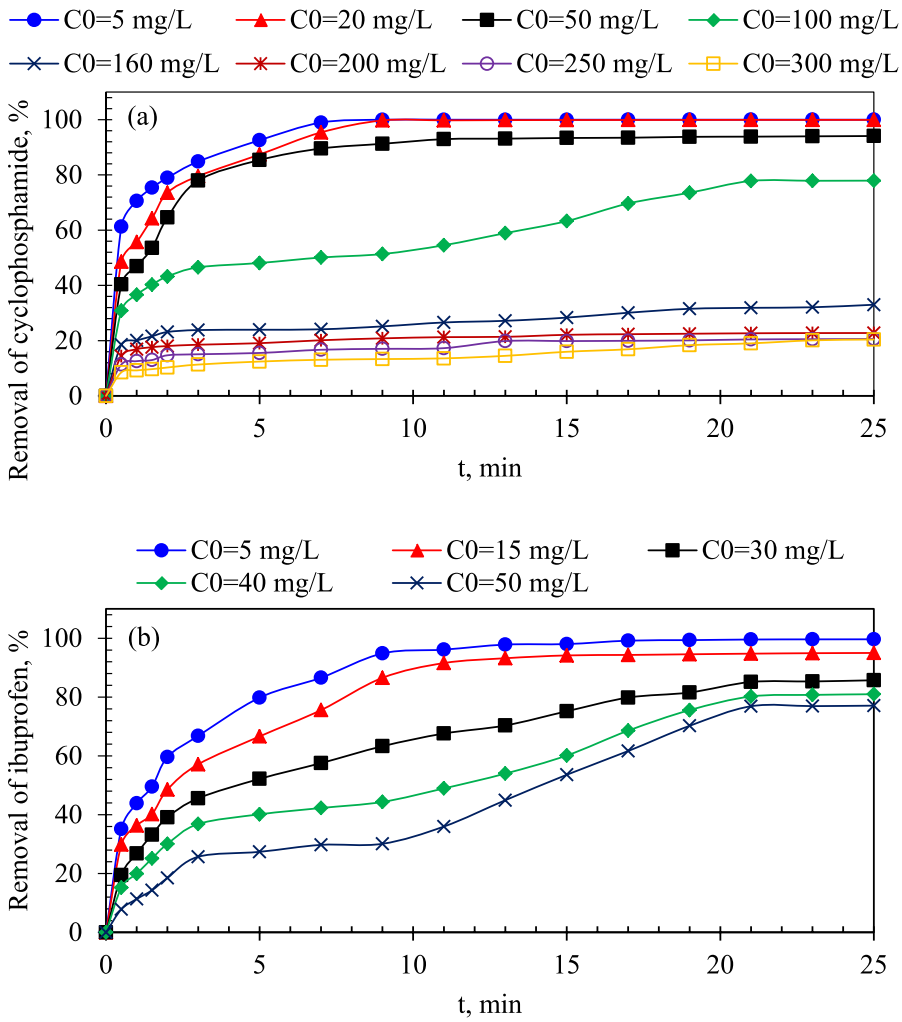

Fig. 14 Effect of time and initial concentration on pollutants removal by AC@$CuFe_2O_4$@MCM-41@GQD; **a** cyclophosphamide (pH = 5, M = 0.5 g/L, and T = 25 °C), **b** ibuprofen (pH = 5, M = 0.5 g/L, and T = 25 °C)

Also, the removal and degradation efficiency of ibuprofen was investigated under the optimal conditions (pH = 5, C_0 = 20 mg/L, M = 0.5 g/L, and T = 25 °C) and using different adsorbents and light conditions (in the presence of a solar lamp/dark box). As shown in Fig. 15b, using the synthesized composite in the presence of a solar lamp, the removal and degradation efficiency of ibuprofen reached about 96%. Meanwhile, when using the synthesized composite in a dark box, the removal and destruction efficiency decreases by 10–15%. For the adsorption of this pollutant (ibuprofen) by the activated carbon in the dark box, the adsorption efficiency decreased by about 20%. Also, under similar conditions, photocatalytic layers ($CuFe_2O_4$@MCM-41) have been investigated in the presence/absence of light. The results show a decrease in the degradation efficiency of ibuprofen compared to the AC@$CuFe_2O_4$@MCM-41@GQD composite (80–85% reduction in the dark box and 40–45% reduction in the presence of a solar lamp).

Effect of competing compounds in wastewater on the efficiency of pollutant adsorption and degradation

To more accurately and competitively investigate the potential of the adsorbent-photocatalyst composite in the removal and degradation of pollutants; competing compounds that occupy the adsorption sites and consume radicals produced by photocatalyst were added to the synthetic wastewater. In this study, the selection of scavengers was based on the dominant reactive species involved in the degradation mechanism of each pollutant as well as their physicochemical differences. To clarify the selection of scavengers, Na-EDTA was used for cyclophosphamide because this compound can strongly compete for metal-coordination sites, allowing us to examine the importance of the initial adsorption step, which is more critical for this highly polar and phosphorylated molecule. Tert-butyl alcohol, ascorbic acid, and chloroform were used

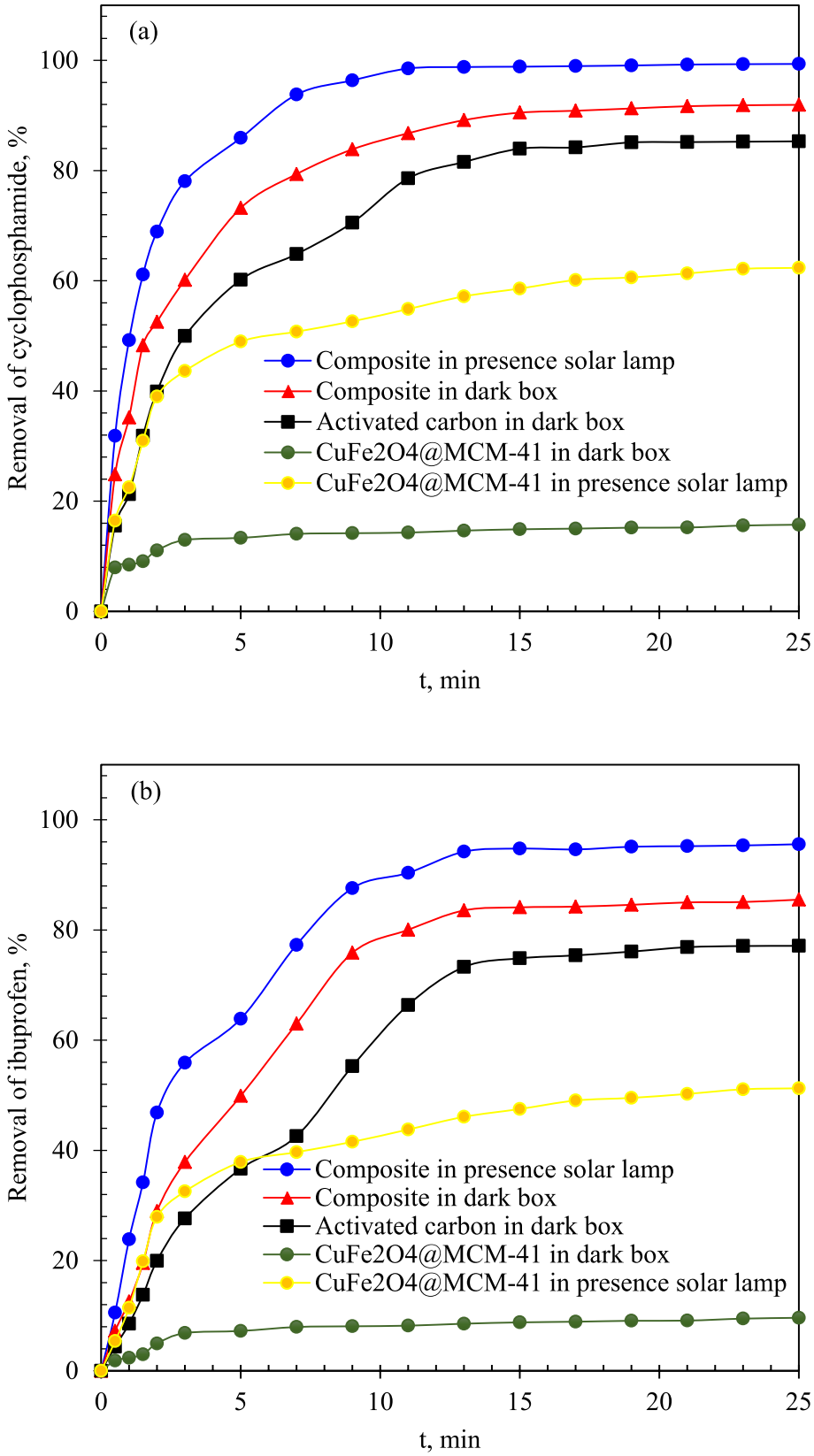

Fig. 15 Effect of time and light on pollutants removal; **a** cyclophosphamide (pH = 5, C_0 = 40 mg/L, M = 0.5 g/L, and T = 25 °C), **b** ibuprofen (pH = 5, C_0 = 20 mg/L, M = 0.5 g/L, and T = 25 °C)

to investigate the roles of hydroxyl radicals, superoxide radicals, and electrons in cyclophosphamide degradation. For ibuprofen, the applied scavengers differed because its degradation pathway relies more on oxidation by photogenerated holes (h^+) and ·OH radicals rather than on pre-adsorption. Therefore, silver nitrate, ammonium oxalate, and tert-butanol were selected to target electrons, photogenerated h^+, and hydroxyl radicals, respectively. It is important to note that ammonium oxalate is a h^+ scavenger, not a proton (H^+) scavenger, and it was used here to probe the involvement of h^+ in ibuprofen oxidation. Figure 16 shows the effect of different compounds added to the wastewater on the pollutant removal and degradation efficiency. The concentration of each compound added to the wastewater is 0.1 M. In Fig. 16a, the results of the removal and photocatalytic degradation of cyclophosphamide in the presence of Na-EDTA (as the adsorption site occupant), tert-butyl alcohol (·OH consuming agent), ascorbic acid ($\cdot O_2^-$ consuming agent), and chloroform (electron consuming agent) as competing compounds in synthetic wastewater and affecting the functional efficiency of the pollutant are shown (Janssens et al. 2019; Zandipak et al. 2020).

The results showed that superoxide radicals and electrons were the main reactive species contributing to cyclophosphamide degradation, which is consistent with its chlorinated oxy-phosphorus structure. The earlier reference to H^+ as a reactive species has been corrected, since H^+ is not generated or scavenged in this context; rather, the relevant species are e^- and $\bullet O_2^-$. Due to its anionic, radical, and redox nature, $\cdot O_2^-$ is capable of reacting with a variety of adsorption-photocatalytic compounds. Although nucleophilic processes and electron transfer reduction seem to be the dominant and effective reaction

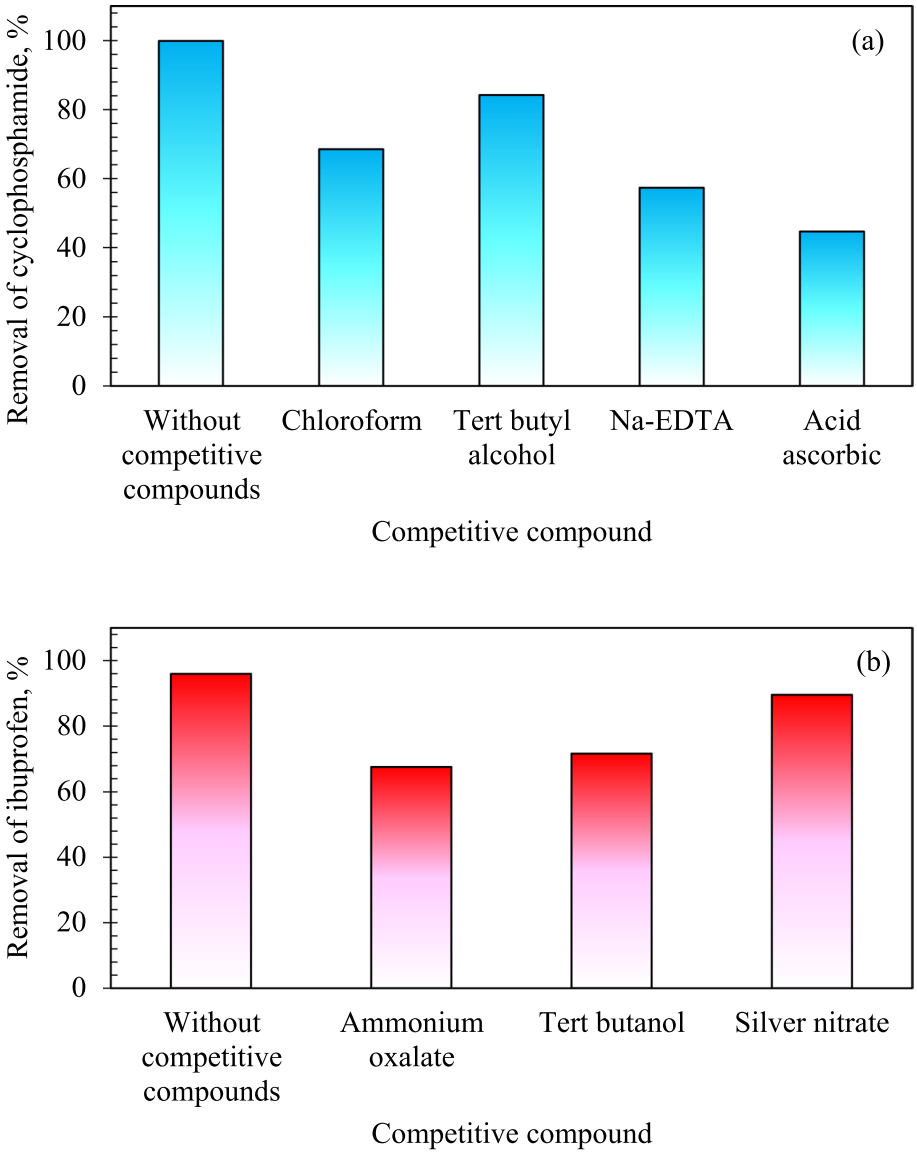

Fig. 16 Effect of various competitive compounds on pollutants removal by AC@$CuFe_2O_4$@MCM-41@GQD; **a** cyclophosphamide (pH = 5, C_0 = 40 mg/L, M = 0.5 g/L, t = 8 min, and T = 25 °C), **b** ibuprofen (pH = 5, C_0 = 20 mg/L, M = 0.5 g/L, t = 9 min, and T = 25 °C)

pathways. Considering that cyclophosphamide is a chlororganic oxy phosphorous derivative, reaction with $\cdot O_2^-$ as well as degradation by electrons is possible, as presented below (Janssens et al. 2019; Zandipak et al. 2020):

$$RCH_2Cl + \cdot O_2^- \rightarrow RCH_2OO \cdot + Cl^- \quad (2)$$

$$RCH_2Cl + 2e^- + H^+ \rightarrow RCH_3 + Cl^- \quad (3)$$

Depending to the characteristics of each compound added to the synthetic wastewater, the removal and destruction efficiency of cyclophosphamide is somewhat reduced. A reduction of between 15–55% was shown in its results.

Figure 16b shows the effect of the presence of silver nitrate, ammonium oxalate, and tert-butanol as e^-, h^+, and •OH scavengers, respectively, on the removal efficiency and photocatalytic degradation of ibuprofen. Among these compounds, silver nitrate had a small effect on the adsorption-photocatalytic performance of the composite compared with ammonium oxalate and tert-butanol, indicating that e^- plays a small role in the removal and degradation of ibuprofen, while h^+ and •OH are more influential. Among h^+ and •OH, •OH plays a more vital role in the photocatalytic degradation process because •OH is the main oxidizing species responsible for the degradation of ibuprofen from the pollutant aqueous solution. The reduction in ibuprofen removal efficiency in the presence of these compounds was 12–30% (Kumar et al. 2018).

The presence of competing compounds in the wastewater solution reduces the removal efficiency by consuming the effective factors in photocatalytic degradation under light radiation and also by occupying the spaces available for pollutant adsorption. These results also demonstrate that the effect of each scavenger is pollutant-specific, reflecting the distinct degradation mechanisms of cyclophosphamide and ibuprofen. This simulation provides a suitable approximation to investigate the potential of the synthesized composite and is close to the real conditions.

Reusability of adsorption-photocatalytic composite

In this study, the adsorbent-photocatalyst composite was reused under optimized process parameters for the removal of pharmaceutical pollutants. After each experiment, the composite was separated from the treated effluent and washed with 0.1 M NaOH. After washing with NaOH, washing with hot distilled water was continued several times. After drying, the remaining material is ready for subsequent reuse. According to the results in Fig. 17, for the removal and elimination of cyclophosphamide, the composite showed a significant decrease in efficiency after the 6th cycle. Also, in the removal and degradation process of ibuprofen after cycle 5, a clear decrease in efficiency was observed (Mondol et al. 2021; Wang et al. 2019).

The decrease in efficiency during the reuse cycles is due to the destruction of the composite structure. This change and degradation of the structure is observed in the analysis of the adsorbent properties (see Figs. 18 and 19).

Examination of real wastewater from the hospital

To understand the potential of the composite synthesized in this study and also to bring the laboratory conditions closer to the real conditions, a sample of hospital wastewater was used to conduct several tests. This wastewater was obtained from Imam Reza Hospital in Kermanshah, Iran. The characteristics of this wastewater are given in Table 4. The reduction of chemical oxygen demand (COD) and total

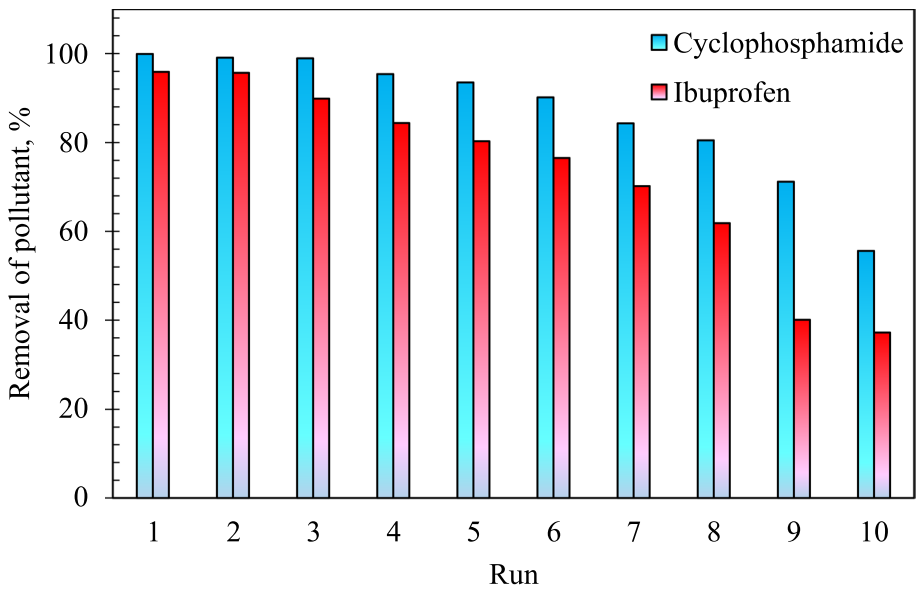

Fig. 17 Results of adsorbent recovery in the process of pollutant removal from wastewater under optimal operating conditions (for cyclophosphamide: pH = 5, C_0 = 40 mg/L, M = 0.5 g/L, t = 8 min, and T = 25 °C; for ibuprofen: pH = 5, C_0 = 20 mg/L, M = 0.5 g/L, t = 9 min, and T = 25 °C)

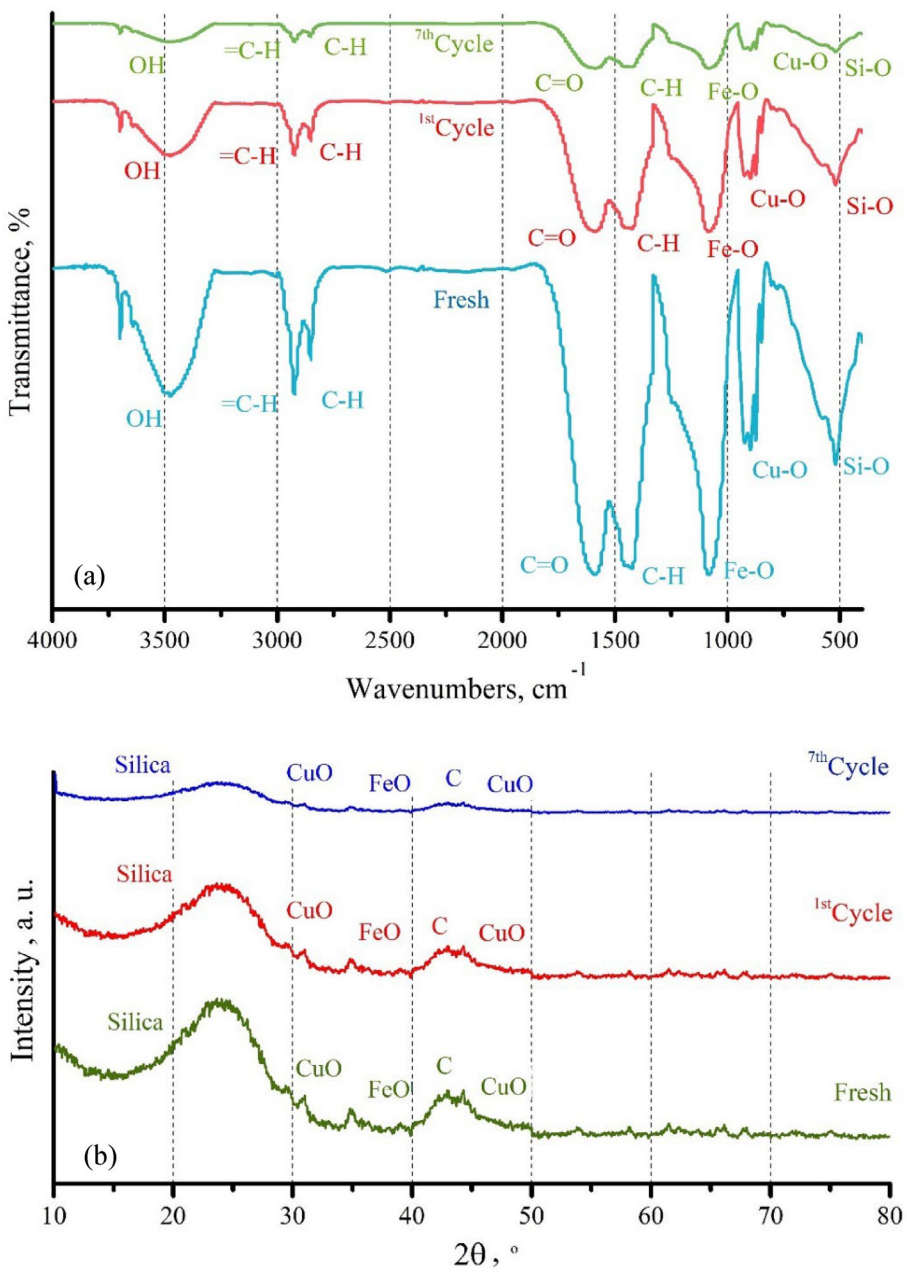

Fig. 18 **a** FT-IR spectra, and **b** XRD pattern for fresh composite, the used composite after the 1st cycle and the used composite after the 7th cycle

organic carbon (TOC) of this wastewater was investigated under constant process conditions and by changing time and composite concentration.

As the plots in Fig. 20a show, the removal rates of COD and TOC increase with time, resulting in removal efficiencies of over 90% for COD and about 77% for TOC. Also, the effect of composite concentration in the range of 0.1–1 g/L on the removal of COD and TOC from hospital wastewater was examined (see Fig. 20b). The results show a significant increase in COD and TOC removal efficiency, indicating the high capacity of the synthesized composite to reduce a variety of harmful environmental pollutants. At a composite concentration of 1 g/L, the COD and TOC removal rates reached about 98% and 82%, respectively. This acceptable removal efficiency demonstrates the high potential of the synthesized composite in reducing harmful environmental parameters of real wastewater.

Conclusion

Due to the scarcity of water resources and the increase in pollution released by humans and related industries, the need to purify and restore water resources has become a concern in today's world. Pharmaceutical pollutants enter water resources in various ways, and various treatment methods

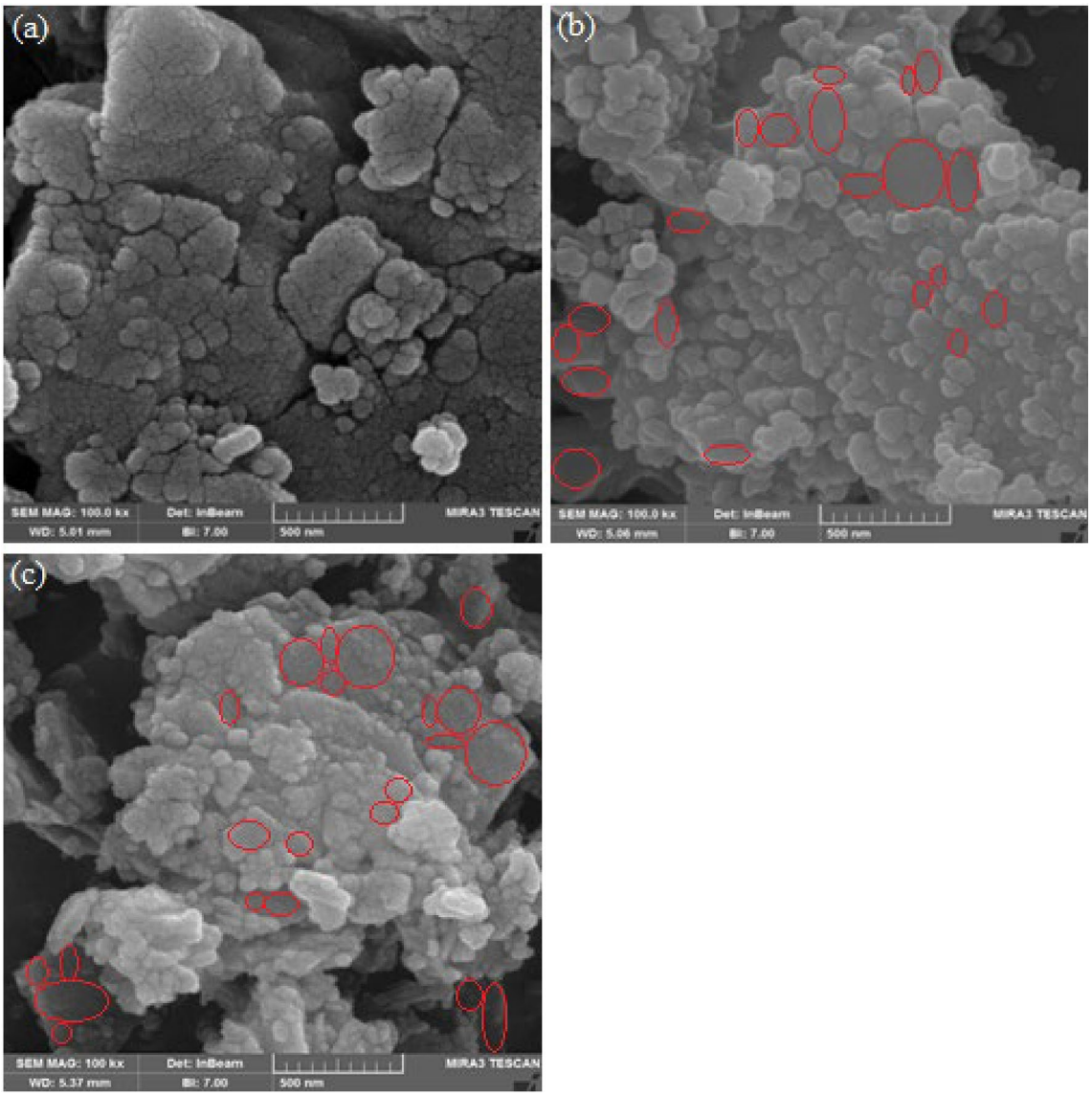

Fig. 19 SEM images of synthesized composite; **a** fresh composite, **b** used composite after the 1st cycle, and **c** used composite after the 7th cycle

Table 4 Physicochemical characteristics of the studied hospital wastewater

Property	Unit	Results
pH	–	7.5
COD	mg/L	765.7
BOD_5	mg/L	482.5
TOC	mg/L	24.3
DOC	mg/L	15.4
TSS	mg/L	58.3
Phosphate	mg/L	15.1
Nitrate	mg/L	16.7
Sulfate	mg/L	287.5

have been developed for their removal. The use of composites that combine adsorption and photocatalytic degradation provides the advantage of integrating two complementary processes into a single treatment step. In this study, a cost-effective and environmentally friendly adsorbent–photocatalyst composite derived from sesame oil meal was synthesized and successfully applied for the simultaneous removal of cyclophosphamide and ibuprofen.

The synthesized AC@$CuFe_2O_4$@MCM-41@GQD composite was fully characterized using EDX, FT-IR, XRD, FESEM, UV–vis DRS, and BET analyses. The effects of operating parameters including pH (2–10), composite dosage (0.1–1 g/L), initial pollutant concentration (5–300 mg/L for cyclophosphamide and 5–50 mg/L for ibuprofen), reaction time (0.5–25 min), and temperature

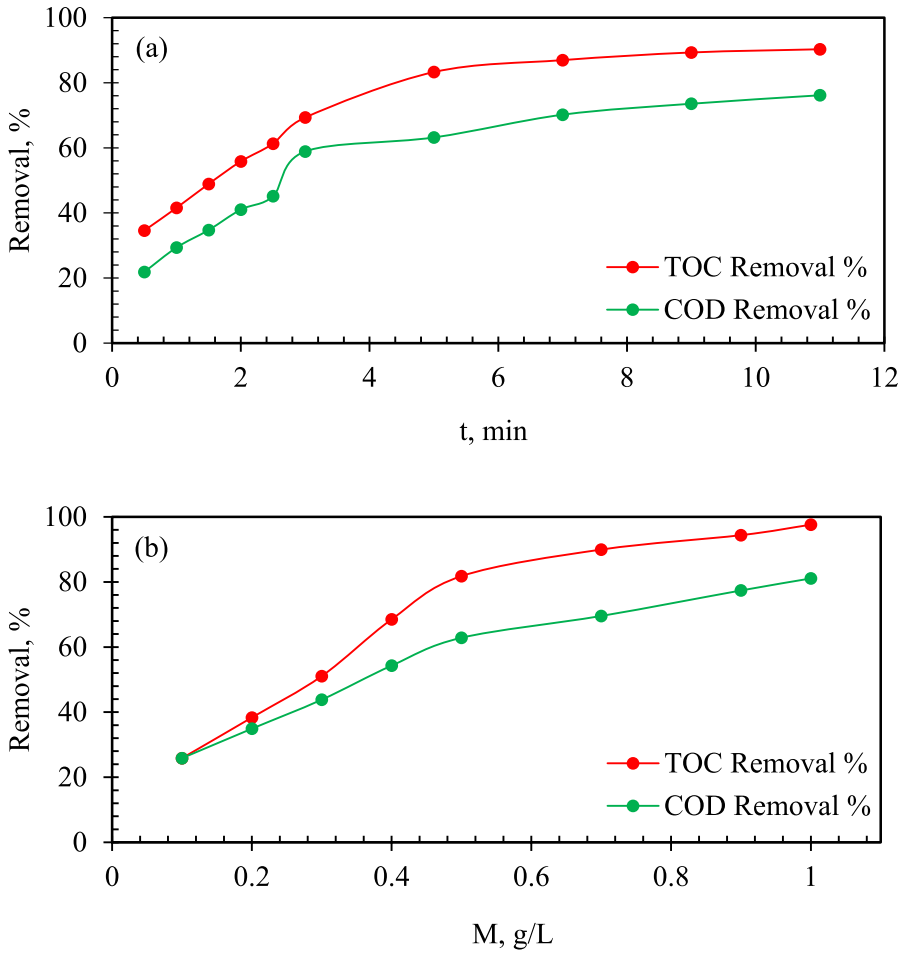

Fig. 20 **a** Effect of time on COD and TOC removal from hospital wastewater (T = 25 ºC and M = 0.5 g/L), **b** effect of composite concentration on COD and TOC removal from hospital wastewater (T = 25 ºC and t = 5 min)

(25–45 °C) were systematically investigated. Under optimized conditions, the composite achieved approximately 100% removal of cyclophosphamide and 98.5% removal of ibuprofen, demonstrating strong synergistic adsorption–photocatalytic activity.

The stability and reusability assessment showed that the composite maintained high performance for several cycles, with efficiency decline becoming significant after the 6th–7th reuse cycle. This reduction correlated well with the structural degradation observed in SEM images. Furthermore, the presence of competing compounds caused a moderate decrease in performance, indicating the sensitivity of reactive species consumption but also confirming the composite's applicability under more complex wastewater conditions.

Finally, evaluation using real hospital wastewater demonstrated substantial reductions in COD and TOC, highlighting the practical applicability and high treatment potential of the synthesized composite. Overall, this study demonstrates that the waste-derived AC@$CuFe_2O_4$@MCM-41@GQD composite is an effective, stable, and sustainable material for pharmaceutical pollutant removal within microphotoreactor systems, offering strong promise for real-world wastewater treatment applications.

Acknowledgement The authors appreciate the support of the Ferdowsi University of Mashhad, Iran (Grant No. 55076) for this work.

Authors contributions Ashkan Gouran: Data curation, Software, Writing—Original draft preparation, Investigation. Ali Ahmadpour: Supervision, Methodology, Writing—Reviewing and Editing. Majid Mohadesi: Supervision, Methodology, Writing—Reviewing and Editing.

Data availability All data, models, or code generated or used during the study are available in a repository or online.

Declarations

Conflict of interest The authors declare that they have no known conflict of interests or personal relationships that could have appeared to influence the work reported in this paper.

Consent for publication Not applicable.

Ethics approval Not applicable.

References

Abegunde SM, Idowu KS (2023) Enhanced adsorption of methylene blue dye from water by alkali-treated activated carbon. Eurasian J Sci Technol 3(3):109–124. https://doi.org/10.48309/ejst.2023.379937.1078

Ahmadi Y, Manafi Moghadam M, Ramazani A (2025) Theoretical insights into alizarin-carbazole dyes for improved DSSC performance using DFT/TD-DFT. Chem Methodol 9(8):702–714. https://doi.org/10.48309/chemm.2025.513306.1920

Ahmadpour A, Do D (1996) The preparation of active carbons from coal by chemical and physical activation. Carbon 34(4):471–479

Ahmadpour A, Do D (1997) The preparation of activated carbon from macadamia nutshell by chemical activation. Carbon 35(12):1723–1732

Al Bahri M, Calvo L, Gilarranz MA, Rodríguez JJ (2012) Activated carbon from grape seeds upon chemical activation with phosphoric acid: application to the adsorption of diuron from water. Chem Eng J 203:348–356

Alamir A, Reidh Abass R, Salah OH, Karim MM, Ahjel S, Al-shuwaili SJ, Kadhim WD, Ahmed RA (2024) Photocatalytic degradation of amoxicillin drug using ZnO/CdS nanocomposite for aqueous solutions by using aops. Adv J Chem, Sect A 7(4):438–447. https://doi.org/10.48309/ajca.2024.449003.1501

Borzyszkowska AF, Pieczyńska A, Ofiarska A, Nikiforow K, Stepnowski P, Siedlecka EM (2016) Bi-B-TiO_2-based photocatalytic decomposition of cytostatic drugs under simulated sunlight treatments. Sep Purif Technol 169:113–120

Budinova T, Ekinci E, Yardim F, Grimm A, Björnbom E, Minkova V, Goranova M (2006) Characterization and application of activated carbon produced by H_3PO_4 and water vapor activation. Fuel Process Technol 87(10):899–905

Constantin LA, Cristea I, Nitoi I, Constantin MA, Nechifor G (2017) Kinetics of cyclophosphamide and ifosfamide degradation from aqueous system via TiO_3 assisted photocatalysis. Rev Chim 68(8):1690–1694

Constantin LA, Constantin MA, Nitoi I, Chiriac FL, Pascu LF, Galaon T (2018) Possible pathway for ifosfamide degradation via Fe-TiO_2 assisted photo catalysis. Rev Chim 69(11):3234–3237

da Costa Borges Soares M, Barbosa FF, Torres MAM, Pergher SB, Essayem N, Braga TP (2021) Preferential adsorption of CO_2 on cobalt ferrite sites and its role in oxidative dehydrogenation of ethylbenzene. Braz J Chem Eng 38(3):495–510

Di G, Zhu Z, Zhang H, Zhu J, Lu H, Zhang W, Qiu Y, Zhu L, Küppers S (2017) Simultaneous removal of several pharmaceuticals and arsenic on Zn–Fe mixed metal oxides: combination of photocatalysis and adsorption. Chem Eng J 328:141–151

Dong Y, Shao J, Chen C, Li H, Wang R, Chi Y, Lin X, Chen G (2012) Blue luminescent graphene quantum dots and graphene oxide prepared by tuning the carbonization degree of citric acid. Carbon 50(12):4738–4743

Ezeokol ED, Josiah PA, Ayeni LA, Olope OI, Afuape AR, Menankiti DT, Ebite C, Donatus UD, Adams A, Osarenren E, Agbalaja RA, Akanbi OS, Ogunmola IO, Majekodunmi AM, Ayomide AA (2024) Synthesis of porous activated carbon derived from biomass-based feedstocks for high performance electrochemical capacitors. Adv J Chem, Sect B Nat Prod Med Chem 6(3):226–246. https://doi.org/10.48309/ajcb.2024.471020.1239

Gashtasbi F, Yengejeh RJ, Babaei AA (2018) Photocatalysis assisted by activated-carbon-impregnated magnetite composite for removal of cephalexin from aqueous solution. Korean J Chem Eng 35:1726–1734

Gogoi A, Mazumder P, Tyagi VK, Chaminda GT, An AK, Kumar M (2018) Occurrence and fate of emerging contaminants in water environment: a review. Groundw Sustain Dev 6:169–180

Gu Y, Yperman J, Carleer R, D'Haen J, Maggen J, Vanderheyden S, Vanreppelen K, Garcia RM (2019) Adsorption and photocatalytic removal of Ibuprofen by activated carbon impregnated with TiO_2 by UV–Vis monitoring. Chemosphere 217:724–731

Guo Y, Rockstraw DA (2007a) Activated carbons prepared from rice hull by one-step phosphoric acid activation. Microporous Mesoporous Mater 100(1–3):12–19

Guo Y, Rockstraw DA (2007b) Physicochemical properties of carbons prepared from pecan shell by phosphoric acid activation. Bioresour Technol 98(8):1513–1521

Haghgoo AA, Cheraghi M, Sobhanardakani S, Lorestani B, Izadkhah V (2023) Preparation of AC/KOH and AC/Fe_3O_4/ZnO nanocomposite from waste rice straw for the removal of cyclophosphamide from aqueous solutions. Toxin Rev 42(1):275–284

Hesas RH, Arami-Niya A, Daud WMAW, Sahu J (2013) Preparation and characterization of activated carbon from apple waste by microwave-assisted phosphoric acid activation: application in methylene blue adsorption. BioResources 8(2):2950–2966

İzgi MS, Saka C, Baytar O, Saraçoğlu G, Şahin Ö (2019) Preparation and characterization of activated carbon from microwave and conventional heated almond shells using phosphoric acid activation. Anal Lett 52(5):772–789

Janssens R, Cristóvão BM, Bronze MR, Crespo JG, Pereira VJ, Luis P (2019) Photocatalysis using UV-A and UV-C light sources for advanced oxidation of anti-cancer drugs spiked in laboratory-grade water and synthetic urine. Ind Eng Chem Res 59(2):647–653

Jermy BR, Ravinayagam V, Alamoudi WA, Almohazey D, Dafalla H, Allehaibi LH, Baykal A, Toprak MS, Somanathan T (2019) Targeted therapeutic effect against the breast cancer cell line MCF-7 with a $CuFe_2O_4$/silica/cisplatin nanocomposite formulation. Beilstein J Nanotechnol 10(1):2217–2228

Jermy BR, Almohazey D, Alamoudi W, Palanivel R, AlSudairi N, Dafalla H, Almofleh A, Alfareed T, Ravinayagam V (2021) Synergistic action of curcumin and cisplatin on spinel ferrite/hierarchical MCM-41 nanocomposite against MCF-7, HeLa and HCT 116 cancer cell line. Cancer Nanotechnol 12(1):33

Jiang Z, Zhang X, Yuan Z, Chen J, Huang B, Dionysiou DD, Yang G (2018) Enhanced photocatalytic CO2 reduction via the synergistic effect between Ag and activated carbon in TiO_2/AC-Ag ternary composite. Chem Eng J 348:592–598

Khan M, Fung CS, Kumar A, Lo IM (2019) Magnetically separable BiOBr/Fe_3O_4@ SiO_2 for visible-light-driven photocatalytic degradation of ibuprofen: mechanistic investigation and prototype development. J Hazard Mater 365:733–743

Khan MI, Singh A, Kumar V, Parashar T, Gairola N, Bhatt SP, Singh K, Jakhmola V (2025) Composition and application of liposome as a carrier for cancer therapy. Chem Rev 7(4):706–728. https://doi.org/10.48309/jcr.2025.519052.1445

Kumar A, Khan M, Zeng X, Lo IM (2018) Development of g-C_3N_4/TiO_2/Fe_3O_4@ SiO_2 heterojunction via sol–gel route: a magnetically recyclable direct contact Z-scheme nanophotocatalyst for enhanced photocatalytic removal of ibuprofen from real sewage effluent under visible light. Chem Eng J 353:645–656

Lai WW-P, Lin HH-H, Lin AY-C (2015) TiO_2 photocatalytic degradation and transformation of oxazaphosphorine drugs in an aqueous environment. J Hazard Mater 287:133–141

Lashaki MJ, Ziaei-Azad H, Sayari A (2022) Unprecedented improvement of the hydrothermal stability of amine-grafted MCM-41 silica for CO_2 capture via aluminum incorporation. Chem Eng J 450:138393

Lestari RA, Elma M, Syauqiah I, Bilad MR, Rahma A (2025) Modification of polyamide thin film-based membranes for water separation: a review. Chem Rev 7(4):674–705. https://doi.org/10.48309/jcr.2025.521927.1453

Li J, Sun S, Qian C, He L, Chen KK, Zhang T, Chen Z, Ye M (2016) The role of adsorption in photocatalytic degradation of ibuprofen

under visible light irradiation by BiOBr microspheres. Chem Eng J 297:139–147
Lim WC, Srinivasakannan C, Balasubramanian N (2010) Activation of palm shells by phosphoric acid impregnation for high yielding activated carbon. J Anal Appl Pyrolysis 88(2):181–186
Lin HH-H, Lin AY-C (2014) Photocatalytic oxidation of 5-fluorouracil and cyclophosphamide via UV/TiO_2 in an aqueous environment. Water Res 48:559–568
Lin AY-C, Hsueh JH-F, Hong PA (2015) Removal of antineoplastic drugs cyclophosphamide, ifosfamide, and 5-fluorouracil and a vasodilator drug pentoxifylline from wastewaters by ozonation. Environ Sci Pollut Res Int 22:508–515
Martins AC, Cazetta AL, Pezoti O, Souza JR, Zhang T, Pilau EJ, Asefa T, Almeida VC (2017) Sol–gel synthesis of new TiO_2/activated carbon photocatalyst and its application for degradation of tetracycline. Ceram Int 43(5):4411–4418
Mazierski P, Białk-Bielińska A, Siedlecka E, Zaleska-Medynska A, Pieczyńska A (2023) Role of operating parameters in photoelectrocatalytic degradation of anticancer drugs: Ifosfamide, 5-fluorouracil and imatinib using CdS/TiO_2. J Water Process Eng 51:103460
Mohadesi M, Gouran A, Seifi K (2022) Removal of ibuprofen from synthetic wastewater using photocatalytic method in the presence of FeO photocatalyst supported on modified Iranian clinoptilolite. Environ Sci Pollut Res Int 29(23):34338–34348
Mohadesi M, Gouran A, Darabi F, Samimi M (2024) Sunflower seed pulp ash as an efficient and eco-friendly adsorbent for Congo red uptake: characteristics, kinetics, and optimization. Water Pract Technol 19(1):228–240
Mondol B, Sarker A, Shareque A, Dey SC, Islam MT, Das AK, Shamsuddin SM, Molla MAI, Sarker M (2021) Preparation of activated carbon/TiO_2 nanohybrids for photodegradation of reactive red-35 dye using sunlight. Photochem 1(1):54–66
Nahil MA, Williams PT (2012) Pore characteristics of activated carbons from the phosphoric acid chemical activation of cotton stalks. Biomass Bioenergy 37:142–149
Nouri Mollalar M, Banaei A, Massoudi A (2025) Synthesis, characterization, and adsorption studies of functionalized graphene oxide via covalent interactions. Chem Methodol 9(9):771–789. https://doi.org/10.48309/chemm.2025.512176.1916
Obasi DE, Ajayi MF, Chimezie NN, Afuape AR, Udoisoh MG, Edun OJ, Ezeoma CC, Aiso SU, Menankiti DT, Oluchukwu AG, Akemu IE, Donatus UD, Allan-Gyimah C, Njoku CO, Ojeniran JI (2024) Optimization of pharmaceutical wastewater treatment using Tiger Nut and TiO_2: a comparative study of photocatalytic degradation and adsorption efficiency. Prog Chem Biochem Res 8(1):1–21. https://doi.org/10.48309/pcbr.2025.456435.1353
Ofiarska A, Pieczyńska A, Borzyszkowska AF, Stepnowski P, Siedlecka EM (2016) Pt–TiO_2-assisted photocatalytic degradation of the cytostatic drugs ifosfamide and cyclophosphamide under artificial sunlight. Chem Eng J 285:417–427
Osawa RA, Barrocas BT, Monteiro OC, Oliveira MC, Florêncio MH (2019) Photocatalytic degradation of cyclophosphamide and ifosfamide: effects of wastewater matrix, transformation products and in silico toxicity prediction. Sci Total Environ 692:503–510
Patnukao P, Pavasant P (2008) Activated carbon from Eucalyptus camaldulensis Dehn bark using phosphoric acid activation. Bioresour Technol 99(17):8540–8543
Pham ST, Nguyen BM, Le GH, Sapi A, Mutyala S, Szenti I, Konya Z, Vu TA (2020) Role of Brønsted and Lewis acidic sites in sulfonated Zr-MCM-41 for the catalytic reaction of cellulose into 5-hydroxymethyl furfural. React Kinet Mech Catal 130:825–836
Prahas D, Kartika Y, Indraswati N, Ismadji S (2008) Activated carbon from jackfruit peel waste by H_3PO_4 chemical activation: pore structure and surface chemistry characterization. Chem Eng J 140(1–3):32–42
Qu X, Liu Y, Zhang C, Zhu A, Wang T, Tian Y, Yu J, Xing B, Huang G, Cao Y (2019) Effect of different pretreatment methods on sesame husk-based activated carbon for supercapacitors with aqueous and organic electrolytes. J Mater Sci Mater Electron 30:7873–7882
Raizada P, Kumari J, Shandilya P, Singh P (2017) Kinetics of photocatalytic mineralization of oxytetracycline and ampicillin using activated carbon supported ZnO/$ZnWO_4$. Desalination 79:204–213
Rammal J, Daou A, El Badan D, Abdel Baki Z, Darwich S, Rammal W, Hijazi A (2025) Comparative analysis of natural and synthetic materials for wastewater treatment: plant powders, activated carbon, biochar, zeolite, and nanomaterials. Chem Rev 7(4):566–590. https://doi.org/10.48309/jcr.2025.511327.1421
Salameh S, Abu Khalil H, Alkhatib M, Ayyad I, Chovelon J-M, Ferronato C, Ayyad O, Qurie M (2026) Combined removal of Pemetrexed drug using adsorption and photocatalytic degradation from polluted water. Adv J Chem, Sect A 9(2):155–165. https://doi.org/10.48309/ajca.2026.531785.1874
Samimi M (2025) Synthesis of alginate–based biocomposite containing biomass derived from *Lantana camara* L. stem as a novel biopolymeric sorbent for methylene blue uptake. Chem Methodol 9(11):1054–1068
Samimi M, Amiri K (2024) Zinc alginate beads as an effective biosorbent for the removal of Eosin-B from aquatic solutions: equilibrium, kinetics, and thermodynamic behaviors. Chem Methodol 8(5):351–363
Samimi M, Moghadam H (2024) Investigation of structural parameters for inclined weir-type solar stills. Renew Sustain Energy Rev 190:113969
Shamsuddin M, Yusoff N, Sulaiman M (2016) Synthesis and characterization of activated carbon produced from kenaf core fiber using H_3PO_4 activation. Procedia Chem 19:558–565
Shukla K, Agarwalla S, Duraiswamy S, Gupta RK (2021) Recent advances in heterogeneous micro-photoreactors for wastewater treatment application. Chem Eng Sci 235:116511
Silva CP, Pereira D, Calisto V, Martins MA, Otero M, Esteves VI, Lima DL (2021) Biochar-TiO_2 magnetic nanocomposites for photocatalytic solar-driven removal of antibiotics from aquaculture effluents. J Environ Manage 294:112937
Sohrabnezhad S, Jafarzadeh A, Pourahmad A (2018) Synthesis and characterization of MCM-41 ropes. Mater Lett 212:16–19
Tafreshi GM, Nakhaei M, Tafreshi AM (2024) Assessment and comparison of techniques for eliminating arsenic from potable water. J Agric Sci Eng 6(4):210–217
Taj-Aldeen RA, Alqaraguly MB, Salah OH, Abdulwahid AS, Hanoon TM, Abud Alzahraa ZH, Omran AA (2024) Enhanced photocatalytic performance of ZnO NPs in the presence of solar light and H_2O_2 for degradation of tetracycline from wastewater: optimal conditions for green products. Adv J Chem, Sect A 7(4):396–405. https://doi.org/10.48309/ajca.2024.437914.1483
Tanveer M, Guyer GT, Abbas G (2019) Photocatalytic degradation of ibuprofen in water using TiO_2 and ZnO under artificial UV and solar irradiation. Water Environ Res 91(9):822–829
Wang N, Li X, Yang Y, Guo T, Zhuang X, Ji S, Zhang T, Shang Y, Zhou Z (2019) Enhanced photocatalytic degradation of sulfamethazine by Bi-doped TiO_2 nano-composites supported by powdered activated carbon under visible light irradiation. Sep Purif Technol 211:673–683
Wang M, Cai Y, Zhou B, Yuan R, Chen Z, Chen H (2022) Removal of PFASs from water by carbon-based composite photocatalysis with adsorption and catalytic properties: a review. Sci Total Environ 836:155652
Xu J, Chen L, Qu H, Jiao Y, Xie J, Xing G (2014) Preparation and characterization of activated carbon from reedy grass leaves by chemical activation with H_3PO_4. Appl Surf Sci 320:674–680
Yahya N, Aziz F, Jamaludin N, Mutalib M, Ismail A, Salleh W, Jaafar J, Yusof N, Ludin N (2018) A review of integrated photocatalyst

adsorbents for wastewater treatment. J Environ Chem Eng 6(6):7411–7425

Yakout S, El-Deen GS (2016) Characterization of activated carbon prepared by phosphoric acid activation of olive stones. Arab J Chem 9:S1155–S1162

Yatimzade MH, Ahmadpour A, Ghahramaninezhad M, Sabzevar AM (2024) Optimizing the efficient removal of ibuprofen from water environment by magnetic carbon aerogel: kinetics, isotherms, and thermodynamic studies. J Mol Liq 408:125337

Yilmaz E, Salem S, Sarp G, Aydin S, Sahin K, Korkmaz I, Yuvali D (2020) TiO_2 nanoparticles and C-nanofibers modified magnetic Fe_3O_4 nanospheres (TiO_2@ Fe_3O_4@ C–NF): a multifunctional hybrid material for magnetic solid-phase extraction of ibuprofen and photocatalytic degradation of drug molecules and azo dye. Talanta 213:120813

Zandipak R, Sobhan Ardakani S, Shirzadi A (2020) Synthesis and application of nanocomposite Fe_3O_4@ SiO_2@ CTAB–SiO_2 as a novel adsorbent for removal of cyclophosphamide from water samples. Sep Sci Technol 55(3):456–470

Zeng G, You H, Du M, Zhang Y, Ding Y, Xu C, Liu B, Chen B, Pan X (2021) Enhancement of photocatalytic activity of TiO_2 by immobilization on activated carbon for degradation of aquatic naphthalene under sunlight irradiation. Chem Eng J 412:128498

Zięzio M, Charmas B, Jedynak K, Hawryluk M, Kucio K (2020) Preparation and characterization of activated carbons obtained from the waste materials impregnated with phosphoric acid (V). Appl Nanosci 10:4703–4716

Publisher's Note Springer Nature remains neutral with regard to jurisdictional claims in published maps and institutional affiliations.

Springer Nature or its licensor (e.g. a society or other partner) holds exclusive rights to this article under a publishing agreement with the author(s) or other rightsholder(s); author self-archiving of the accepted manuscript version of this article is solely governed by the terms of such publishing agreement and applicable law.